Contemporary Physics
Vol. 49, No. 3, May–June 2008, 157–178

Taylor & Francis
Taylor & Francis Group

Granular gas dynamics: how Maxwell's demon rules in a non-equilibrium system

Ko van der Weele*

Mathematics Department, University of Patras, Patras, Greece

(*Received 26 February 2008; final version received 18 April 2008*)

The main characteristic of a granular gas, which makes it fundamentally different from ordinary molecular gases, is its tendency to form clusters, i.e. to spontaneously separate into dense and dilute regions. This can be interpreted as a separation in cold and hot regions, meaning that Maxwell's demon is at work: this demon – notoriously powerless in any system in thermodynamic equilibrium – makes clever use of the non-equilibrium state of affairs that reigns in a granular gas, with on the one hand an external energy source and on the other a continuous loss of energy due to the inelastic particle collisions.

We focus on vibrated compartmentalised systems, because these give a particularly clear-cut view of the clustering process and also because they resemble the typical machinery used in industrial applications to sort and transport granular materials. We discuss how the clustering can be exploited to build a Brownian motor, a fountain, a granular clock, and how it gives insight into a related clustering problem of prime importance in modern society, namely the formation of traffic jams.

Keywords: granular gas; clustering; Maxwell's demon; hydrodynamic description; Brownian motor; traffic jams

1. Introduction: why does granular matter matter?

Granular, grain-like matter is all around us. We meet it in our daily lives when we pour sugar, stir coals or walk on a gravel path, and the industrial applications involving this type of matter are so ubiquitous that they use up an awe-inspiring 10% of the energy budget worldwide [1,2]. It has also been estimated that no less than half of this energy could be saved if our understanding of granular matter were more complete [3]: notwithstanding our familiarity with the more practical aspects of grainy materials, on the fundamental side much is still unknown. With the exception of pioneers like Chladni, Faraday, Reynolds, Hagen, and Bagnold [4–6], physicists were not seriously interested in granular matter until about 20 years ago. Since then, however, it has rapidly become one of the most active branches of physics and new discoveries are being made every day.

Just like ordinary molecular matter, granular matter comes in at least three phases: solid (e.g. a sand castle, Figure 1(*a*)), liquid (the flowing sand in an hourglass, Figure 1(*b*)), and gaseous (as in a desert dust devil, Figure 1(*c*)). One also encounters phases that look intermediate between solid and liquid, or between liquid and gas. Despite the superficial similarities, however, granular solids, liquids, and gases differ radically from their molecular counterparts [1]. Used as we are to ordinary matter, we find their behaviour often counterintuitive. For instance, granular *solids* often *dilate* – instead of being compressed – under external pressure or shear. This is due to the fact that the increased pressure disturbs the close-packed arrangement of the grains, forcing them into another arrangement, which usually happens to be a less dense one. It was Osborne Reynolds who first thought of this in 1885, when he was walking along the seaside and wondered why the sand made a white ring around his footprints. He correctly attributed this to the widening voids between the grains, through which the water could drain away with more ease, thus making the sand drier and whiter.

Granular *liquids* are also special. Take for instance the sand in an hourglass, which flows always at the same rate, irrespective of whether the upper vessel is well-filled or nearly empty.[1] For a water clock, by contrast, the flow steadily slows down as the water level in the upper vessel (and hence the hydrostatic pressure at the orifice) decreases. The sand hardly builds up any hydrostatic pressure, since the gravitational force is being re-directed towards the sides of the hourglass via the erratic lines of contact (known as force chains) between the grains.

One of the most distinctive properties of granular *gases* is their tendency to *cluster* [7–12]. Any ordinary gas will spread over the whole volume of the container in which it is held, but a granular gas does exactly the opposite: it forms clusters, i.e. it spontaneously

*Email: weele@math.upatras.gr

ISSN 0010-7514 print/ISSN 1366-5812 online

DOI: 10.1080/00107510802141226
http://www.informaworld.com

separates into dense and dilute regions (see Figure 2). This property, which can be traced back to the fact that the collisions between the grains are inelastic, is the central topic of the present review. We will concentrate on the formation of clusters in *compartmentalised* granular gases. These systems give us a particularly transparent view of the clustering process, and apart from this they also have a direct bearing on the multitude of compartmentalised systems found in industry, such as sorting machines, mixers, and conveyor belts, for which clustering is known to be a major and very costly source of problems [1,2].

The fact that driven granular systems are so widely studied today is due in part to their attractively surprising behaviour, and to their relevance for industrial applications, but there is more to it than that: they are prime examples of many-particle systems far from thermodynamic equilibrium, renowned for their rich phenomenology and complex dynamical properties. In such systems, the balance between energy input on the one side and dissipation on the other is known to give rise to spontaneous pattern formation [13]. Typical instances are the hexagonal convection cells in a pan of oil heated from below (Rayleigh–Bénard cells) [14], the sand ripples along the beach formed by the to-and-fro motion of the sea water [15], or – as we shall see – the spontaneous formation of clusters in granular gases. In the present review we ignore the influence of the medium surrounding the particles. For the systems we will be dealing with (glass or metal beads with a typical diameter of several millimetres, moving in air at atmospheric pressure) this is a fair approximation,[2] but it excludes fascinating granular phenomena like the

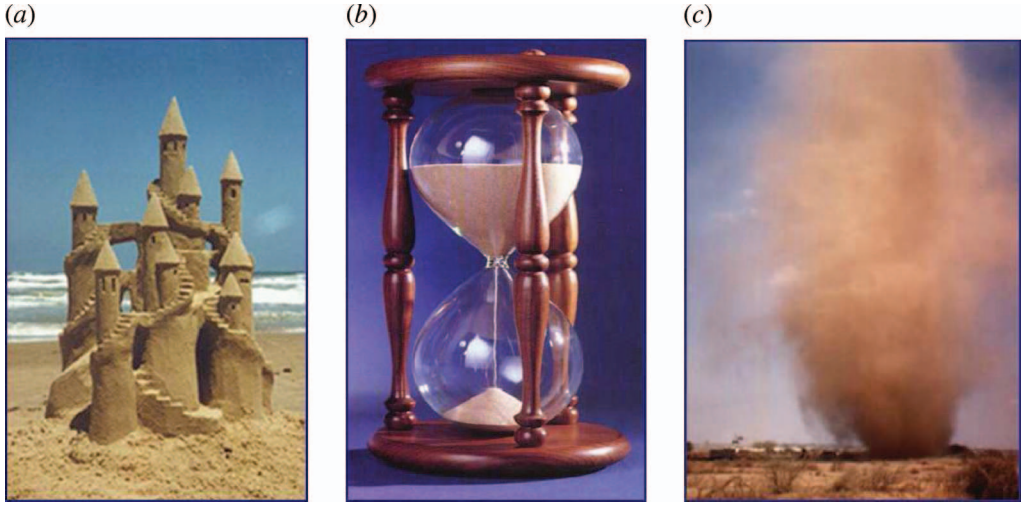

Figure 1. Granular matter as a solid, a liquid, or a gas: (*a*) sand castle, (*b*) hourglass, and (*c*) dust devil. A dust devil is a whirlwind caused by intense heating of the desert surface. The hot air swirls upwards, carrying fine particles of dust and sand with it.

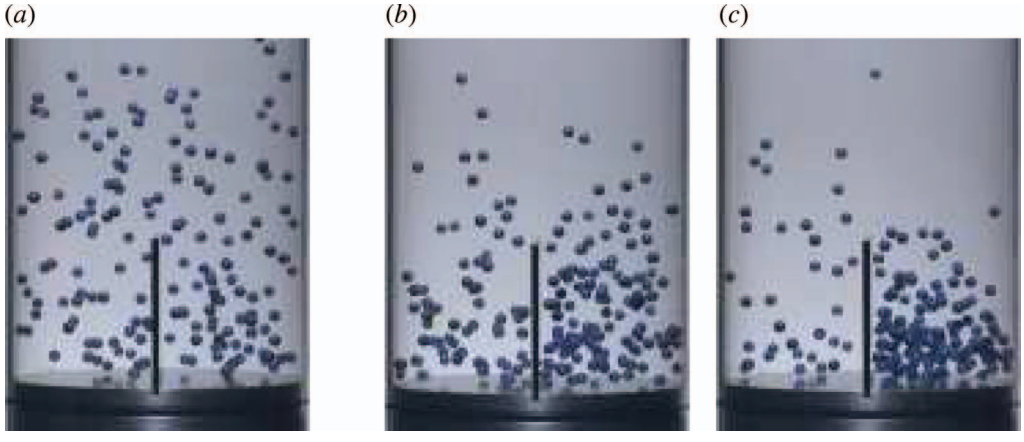

Figure 2. The Maxwell demon experiment: (*a*) at vigorous shaking the particles (glass beads of diameter 4 mm) spread evenly over the two compartments. (*b*,*c*) When the shaking strength is reduced below a critical level, the particles spontaneously form a cluster in one compartment, leaving the other one almost empty. Note that the particles in the dilute compartment jump higher (i.e. the granular temperature T_g is higher) than in the well-filled compartment. The height of the wall is 60 mm.

dust devil of Figure 1(*c*), barchan dunes marching through arid deserts with unidirectional winds (on Earth as well as on Mars and Venus) [6],[3] or the appearance of Faraday heaps in a layer of powder on a vibrating table [5,18,19].

Granular systems are intrinsically noisy, since the phenomena they display typically involve much fewer than the 10^{23} particles of standard statistical physics. This means that statistical fluctuations are not drowned by the law of large numbers, but may in fact play a decisive role in the behaviour of the system.[4] Granular systems are therefore uniquely suited to study the role of statistical fluctuations in non-equilibrium systems.

The paper is organised as follows: Section 2 describes the *Maxwell Demon experiment*, which shows the clustering in its most clear-cut form in a setup consisting of two connected compartments (see Figure 2). Section 3 then deals with the theoretical description of the clustering process. This description is based on *granular hydrodynamics* and yields a *flux function* that quantitatively captures the flow of particles between the two compartments. Section 4 is about the generalisation of the Maxwell demon experiment to three or more compartments, which introduces intriguing new features: the transition from the uniform particle distribution to the clustered state now turns out to be *hysteretic*, and does not occur in one single step but is instead a slow *coarsening* process involving long-lived transient states. In Section 5 we discuss how the clustering effect can be exploited to extract useful work from the granular gas. By making a small adjustment to every second compartment, we induce a directed motion through the system, which thus becomes a *Brownian motor*. Section 6 deals with another interesting variation of the Maxwell Demon experiment: if the granular particles are not all identical, but rather a mixture of small and large particles, the cluster can be made to switch periodically from one compartment to the other. This is called the *granular clock*. Finally, in Section 7 we discuss the close analogy with a clustering problem of great importance in modern society: the spontaneous formation of *traffic jams* on a highway. The clustering of cars bears a strong resemblance to granular clustering and indeed some of the more promising models proposed for its description are similar to the flux model mentioned above.

2. The Maxwell demon experiment

2.1. A misbehaving gas

A striking illustration of cluster formation, known as the Maxwell Demon experiment after the inspiring title of [21], is shown in Figure 2. It consists of a cylindrical container, mounted on a shaker, and divided into two equal compartments by a wall. A handful of millimetre-sized beads are brought into a gaseous state by shaking the system vertically (with amplitude a and frequency f) and are thus able to jump from one compartment to the other over the wall. If the shaking is vigorous, the particles fly throughout the container, distributing themselves equally over the two compartments just as in any ordinary gas (Figure 2(*a*)). Indeed, the beads even show a vertical density profile that resembles the barometric height distribution, falling off more or less exponentially with the height above the vibrating bottom.

However, when the shaking strength is reduced beneath a critical level, the particles are seen to jump preferentially into *one* of the compartments (Figures 2(*b*) and (*c*)).[5] This goes on until a dynamic equilibrium is reached between the two compartments. In this situation, the average outflow of rapid particles from the nearly empty compartment is balanced by the outflow of slow particles from the well-filled compartment.

This experiment was presented by Nordmeier and Schlichting in 1995 [22]. Similar experiments had been carried out before, by high school teachers wishing to demonstrate the properties of a molecular gas, but they had always discarded it as a failure: the setup did not even fulfill the most basic property of all, namely that a gas should spread uniformly over the available space. Schlichting and Nordmeier were the first to recognise the experiment for what it really was, namely an excellent example of a granular gas showing spontaneous cluster formation.

The clustering is a consequence of the inelasticity of the particle collisions (Figure 3) [8]. In every collision, the particles lose some small part of their kinetic energy, and this means that they make each other slow. Stated more precisely, the collisions render their relative velocity smaller, thereby simultaneously decreasing the velocity fluctuations. If one of the

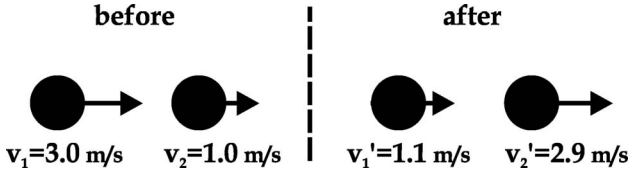

Figure 3. The key to granular clustering: inelastic collision of two identical particles. The sum of the velocities is constant ($v_1+v_2 = v_1'+v_2'$), expressing momentum conservation, whereas their difference becomes smaller by a factor $e = -(v_2'-v_1')/(v_2-v_1)$, called the coefficient of normal restitution. Here we have taken $e = 0.9$, the same value as for the beads in Figure 2. The pair of particles loses a fraction $\varepsilon = (1-e^2)$ of its initial kinetic energy. For $e = 1$ the collision would be fully elastic, and the particles would not show any tendency to cluster together.

compartments contains considerably more particles than the other (as will certainly be the case sooner or later, due to statistical fluctuations) the particles in this compartment will collide more often, become slower, and hence jump less easily over the wall. Vice versa, the particles in the other compartment will jump higher. From this moment on the process becomes a snowball effect: the particles from the underpopulated compartment jump with increasing ease into the dense compartment, and the growing density in the latter makes the particles here slower and slower. So one compartment is diluted while the other one develops a cluster of slow particles, precisely as in Figure 2(*c*).

Only at sufficiently strong shaking the dissipation is overpowered by the energy input, and the fluctuations in the population are destroyed before the cluster has a chance to develop. That is, the particles remain distributed equally over the two compartments.

In terms of the *granular temperature* T_g, i.e. the mean kinetic energy of the particles, the clustering can be interpreted as a separation into a 'cold' compartment (containing a lot of relatively slow particles) and a 'hot' one (containing only a few rapid particles). This is reminiscent of Maxwell's Demon, but in a completely new context, outside of thermodynamic equilibrium [21].

2.2. *Maxwell's demon*

The demon was introduced by James Clerk Maxwell in 1867 in a letter to his friend and colleague Peter Guthrie Tait, and four years later he used it in his *Theory of Heat* to illustrate the statistical nature of the second law of thermodynamics [23,24]. Maxwell envisioned two rooms with a small hole in the wall between them. Initially, the air is in thermodynamic equilibrium throughout the system, so the temperature T in both rooms is equal. A little demon guards the opening in the wall. Its task is simple: to let through only *slow* molecules in one direction, and only *fast* molecules in the opposite direction, and thus create one cold and one hot room.

Maxwell's point was that such a separation of slow and fast molecules requires work. The probability that it would ever happen spontaneously in an ordinary gas consisting of any sizeable number of molecules is vanishingly small, and would in fact be a violation of the second law of thermodynamics – equally improbable as seeing one part of the water in a glass spontaneously come to the boil while the other parts turned into ice. However, the demon which is so powerless in ordinary gases rears its head in the granular experiment of Figures 2(*b*) and (*c*). Of course it does so without violating any law of physics: the granular gas is *not* in thermodynamic equilibrium (it gets a continuous *supply* of energy from the vibrating bottom, which is continuously *dissipated* via the inelastic particle collisions) and the observed clustering is in fact a bona fide example of pattern formation in a non-equilibrium system.

A granular gas without external energy input is destined to come to rest. Also in this case (a *freely cooling* granular gas) one may witness cluster formation. This was demonstrated by Goldhirsch and Zanetti, see Figure 4, who were the first to give a general explanation for clustering in granular gases [8]. They considered a freely cooling granular gas in two dimensions, consisting of a large number of discs (like hockey pucks on a frictionless ice floor) colliding inelastically. The discs were initially spread out homogeneously, with a Maxwellian velocity distribution, and then left to evolve without any further energy input. As a result of the collisions, the mean kinetic energy of the discs (the granular temperature) decreases steadily. Figure 4 shows the situation after 10 million collisions, clearly illustrating the spontaneous formation of dense and dilute regions. The particles in the characteristic string-shaped clusters have practically come to a standstill, whereas those in the dilute regions are still moving about. On a more detailed level, also other things happen (e.g. the

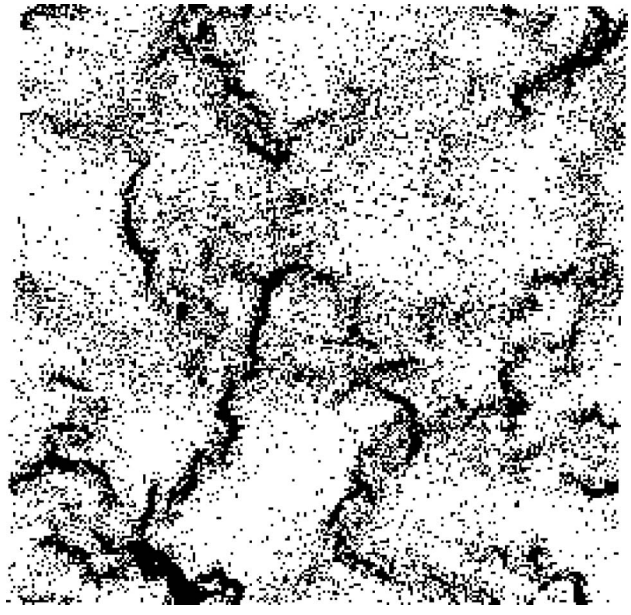

Figure 4. Cluster formation in a simulated freely cooling granular gas, consisting of 40,000 discs colliding inelastically (with restitution coefficient $e = 0.6$) on a frictionless floor. The fraction of the floor area covered by the discs is 0.05, and periodic boundary conditions are used in both directions. The snapshot is taken after 10 million collisions, i.e. on average 500 collisions per particle. From [8]. Reprinted figure with permission from Goldhirsch and Zanetti, Phys. Rev. Lett., 70, 1619, 1993. Copyright (1993) by the American Physical Society.

velocity distribution develops a non-Maxwellian tail [11,12], and certain strings of particles may experience an inelastic collapse, i.e. an infinite number of collisions in a finite time [25]) but here we will restrict ourselves to the clustering effect.

Since it plays such a crucial role, let us look at the mechanism of energy dissipation in some more detail. Figure 3 depicts a head-on collision of two beads, colliding with a coefficient of normal restitution $e = 0.9$ (like the glass beads in Figure 2): the total momentum of the two beads is conserved during the collision, but their relative velocity is diminished by a factor 0.9. The centre-of-mass kinetic energy after the collision is therefore only 0.81 ($= e^2$) of its value before the collision. Nineteen percent is transferred to the microscopic energy scales in the form of deformations, heat, and sound. But why does this mean that it is effectively lost?

Taking the situation of Figure 2(*a*), the typical kinetic energy of a glass bead with radius 4 mm (i.e. mass $m \approx 10^{-4}$ kg) and speed $v \approx 1\ \mathrm{ms}^{-1}$ is $\frac{1}{2}mv^2 \approx 0.5 \times 10^{-4}$ J. This is to be compared with the typical microscopic energy scale $k_\mathrm{B}\,T \approx 0.4 \times 10^{-20}$ J at room temperature $T \approx 300$ K, with $k_\mathrm{B} = 1.38 \times 10^{-23}$ J K^{-1} the Boltzmann constant. The enormous gap between these two energy scales – sixteen orders of magnitude! – means that the energy transferred to the microscopic levels will never be returned in any coherent fashion so as to contribute to the bead's kinetic energy. *This* is the crucial difference with ordinary molecular gases, where the kinetic, vibrational, and rotational energy scales are all of the same order ($\sim k_\mathrm{B}T$), enabling a continuous exchange between them. In a granular gas, room temperature is by no means enough to stir the particles thermally and for this reason the gas is sometimes called *a-thermal*: the normal temperature T is negligible for all practical purposes. That is why we work with the granular temperature T_g instead.

The granular temperature is defined as [11,26–29]

$$T_\mathrm{g}(\boldsymbol{r}, t) = \frac{1}{2}m\langle v^2 - \langle v\rangle^2\rangle, \qquad (1)$$

where the brackets $\langle\,..\,\rangle$ denote an ensemble average (at position $\boldsymbol{r}$ and time t) over many realisations of the experiment under consideration. Just as in the kinetic theory of ordinary gases, the temperature (1) is related to the fluctuating energy due to the random motion of the particles around the local mean velocity $\langle v\rangle$. It plays the same role – and has the same dimension of energy – as the combination $k_\mathrm{B}T$ in standard statistical physics. Indeed, many of the well-known relations for the thermodynamic temperature can be used (with proper care[6] [30–33]) also in granular dynamics, provided that one takes $k_\mathrm{B} = 1$. An example is the ideal-gas law relating the pressure, density, and temperature of a diluted gas, which we will encounter in the next section (Equation (3)). In the Maxwell Demon experiment, where the mean velocity $\langle v\rangle$ is approximately zero, the temperature $T_\mathrm{g}(\boldsymbol{r}, t)$ defined by Equation (1) may simply be identified with the kinetic energy of the particles at position $\boldsymbol{r}$ and time t.[7]

3. How to model the clustering

3.1. Granular hydrodynamics

Several theoretical models have been proposed to describe the cluster formation in the Maxwell demon experiment. The first one was given by Eggers, who treated the granular gas as a hydrodynamic continuum and derived an expression for the particle flux between the two compartments [21]. Alternative descriptions were given by Lipowski and co-workers [35,36] who pictured the Maxwell demon experiment as a modified version of the Ehrenfest urn model [37], and by Cecconi et al. [38] who treated it as a two-well escape problem in the spirit of Kramers' model for chemical reactions [39,40]. A closely related horizontal version of the Maxwell demon experiment was treated in hydrodynamic terms by Brey et al. [41]. Each of these models has its own merits (for an overview see [42]) but here we choose to focus on Eggers' model, which was historically the first one and stays most closely to the actual experiment.

It also gives us the opportunity to touch upon one of the central themes in the field of granular matter today, namely, the question to what extent the rich variety of phenomena observed in granular systems can be captured by hydrodynamic continuum theory [20,26,43–46]. Such a theory – in which the particles are represented by continuum fields for the density, velocity and temperature – can hardly be expected to cover *all* phenomena, but only those which have a typical length scale that is large compared to the size of the mean free path of the particles. This is certainly not always the case in granular systems, and it is this lack of separation of scales (especially for the small-scale phenomena) which forms the main obstacle for a general continuum theory of granular matter. Nevertheless, for large-scale collective phenomena hydrodynamic modelling is a natural approach and has been successfully applied to a large number of effects ranging from the prominent anisotropy of the normal stress in granular media [44] and the fluid-like impact of a steel ball on sand [47] to the granular Leidenfrost effect [48,49], the formation of longitudinal vortices in granular chute flows [50,51] and convection rolls in a vibrated granular bed [52,53]. In some of these cases hydrodynamics even works beyond the nominal range of its validity. As we will see, the clustering in compartmentalised granular gases is well described by hydrodynamic theory too.

As a starting point, Eggers took the condition for dynamic equilibrium between the two compartments, namely that the flux of particles from left to right must equal that from right to left:

$$F_{\mathrm{l}\to\mathrm{r}} = F_{\mathrm{r}\to\mathrm{l}}, \tag{2}$$

noting that an asymmetric equilibrium (as in Figure 2(*c*)) can only be explained if the particle flux from a compartment is *not* a monotonically increasing function of the number of particles in the compartment, as it would be for a gas of elastically colliding particles. Instead, it must show a maximum.

Eggers considered a two-dimensional gas of colliding discs, in a setup that really brings to life the thought experiment of Maxwell (even more so than the setup of Figure 2): the wall is taken to extend over the whole height of the system, with only a small opening of width S positioned at height h above the bottom, see Figure 5(*a*). The bottom of the container is taken to move in a sawtooth manner, with amplitude a and frequency f, such that a colliding particle always finds it to move upward with the same velocity $v_b = af$. Moreover, the amplitude a is very small compared to the mean free path of the particles, which means that the bottom is effectively stationary.

Assuming the gas inside each compartment separately to be in a steady state (the flux is assumed to be sufficiently small to justify this), one can derive an analytic expression for the particle outflow from each compartment, based on three hydrodynamic equations.

(1) The equation of state relating the pressure p, number density ρ, and granular temperature T_{g}. Keeping things as simple as possible, Eggers chose the well-known relation for an ideal gas (with $k_{\mathrm{B}} = 1$):

$$p = \rho T_{\mathrm{g}}. \tag{3}$$

Of course, it would be possible to make a more refined approximation by taking into account the excluded volume taken up by the particles (introducing van der Waals-like terms in the equation of state [48,54–56]). However, this is only important in the dense case, when the volume fraction is high. It does not bring any qualitative changes here and we therefore stick to the minimal choice of the ideal gas law (3).

(2) The momentum balance, which indicates how fast the pressure drops with the height z above the bottom:

$$\frac{\mathrm{d}p}{\mathrm{d}z} = -mg\rho, \tag{4}$$

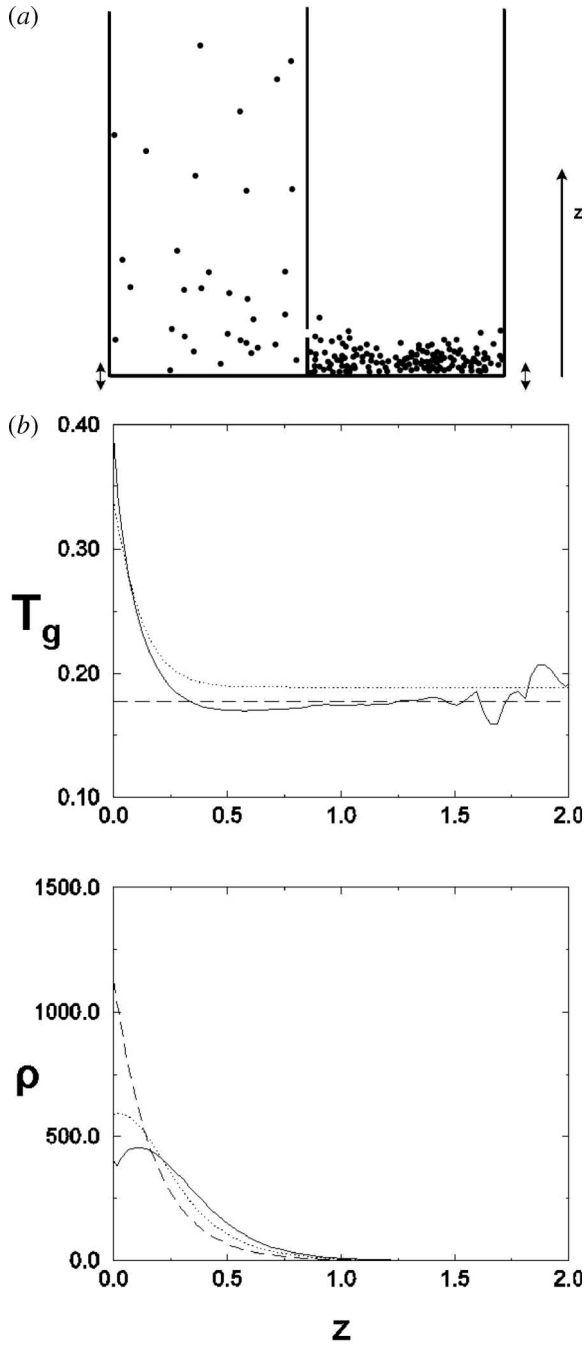

Figure 5. (*a*) The Maxwell demon experiment as envisaged by Eggers. The two compartments communicate through a small opening in the wall, just as in Maxwell's original thought experiment, which is positioned at about 40 particle diameters above the vibrating bottom. (*b*) Granular temperature $T_{\mathrm{g}}(z)$ and particle density $\rho(z)$ in a one-compartment system. The solid lines come from MD simulations for 320 particles in a compartment that is 160 particle diameters wide, colliding with restitution coefficient $e = 0.95$ ($\varepsilon = 0.0975$), the dotted lines represent the hydrodynamic Equations (3)–(5), and the dashed lines the constant-T approximation used in the flux model. One unit along the z-axis corresponds to 50 particle diameters. From [21]. Reprinted figure with permission from J. Eggers, Phys. Rev. Lett., 83, 5322, 1999. Copyright (1999) by the American Physical Society.

where m is the mass of a particle and $g = 9.81\ \mathrm{ms}^{-2}$ is the gravitational acceleration.

(3) The balance between the energy flux through the gas (emanating from the vibrating bottom) and the dissipation due the inelastic particle collisions:

$$\frac{\mathrm{d}}{\mathrm{d}z}\left(T_{\mathrm{g}}^{1/2}\frac{\mathrm{d}T_{\mathrm{g}}}{\mathrm{d}z}\right) = C\varepsilon\rho^2 T_{\mathrm{g}}^{3/2}, \qquad (5)$$

where $\varepsilon = (1-e^2)$ is the inelasticity parameter. The left-hand side is modelled after the standard heat conduction through a gas, $(\mathrm{d}/\mathrm{d}z)\,[\kappa\,(\rho,\,T)\,\mathrm{d}T/\mathrm{d}z]$, with the heat conductivity $\kappa(\rho, T) \propto \rho T^{1/2}\ell(\rho)$ being proportional to the product of the density of the particles, their velocity, and the mean free path length between collisions. The right-hand side represents the energy dissipation rate, which is equal to the energy loss in one collision ($\propto \varepsilon T_{\mathrm{g}}$) times the total number of collisions per unit time ($\propto \rho T_{\mathrm{g}}^{1/2}/\ell(\rho)$) [48,49]. Taking the mean free path length to be reciprocal to the number density as in an ideal gas [$\ell(\rho) \propto 1/\rho$], one arrives at Equation (5). The coefficient $C\,(=\pi d^2$ [21]) is constant in the present context.

Just like the equation of state, also the energy balance (5) can be refined (e.g. by using a more intricate formula for $\kappa\,(\rho,\,T)$ or adding an extra heat conduction term proportional to $\varepsilon T_{\mathrm{g}}{}^{3/2}\mathrm{d}\rho/\mathrm{d}z$ [44]), but again this does not alter the qualitative features of the model. We further note that the energy balance of Equation (5) presupposes that the density of particles in each compartment is sufficiently large to make the inter-particle collisions the dominant source of dissipation. One might expect this to become a problem for the compartment that is diluted, because here the density will sooner or later become so small that the particles hardly meet other particles anymore, and the main source of dissipation will then be the collisions with the walls.[8] The system is then in the Knudsen regime and no longer describable by hydrodynamics. In the corresponding Molecular Dynamics (MD) simulations, Eggers simply took the collisions with the walls to be elastic.

The granular temperature $T_{\mathrm{g}}(z)$ and density $\rho(z)$ that are found on the basis of the three hydrodynamic Equations (3)–(5) are given by the dotted lines in Figures 5(*b*) and (*c*). They agree well with the results of the MD simulations (solid lines). The temperature profile $T_{\mathrm{g}}(z)$ is seen to be close to constant, except for a narrow region close to the bottom; this is the region where the energy is injected into the system and the particles have not yet had the chance to redistribute this energy via collisions. Given that the height $z = h$ at which the hole is positioned lies considerably above this region, it is not unreasonable to approximate the temperature profile with a simple constant: $T_{\mathrm{g}}(z) = T_k$, with $k = 1,\ 2$ labelling the compartments. This approximation is represented by the dashed line in Figures 5(*b*) and (*c*).

Now, substituting the ideal-gas law Equation (3) into Equation (4) one gets $\mathrm{d}(\rho T_{\mathrm{g}})/\mathrm{d}z = -mg\rho$, and within the constant-temperature approximation $T_{\mathrm{g}}(z) = T_k$ this becomes (for each compartment separately) $T_k\ \mathrm{d}\rho_k/\mathrm{d}z = -mg\rho_k$. This is easily solved to give a density profile that decays exponentially with the height above the floor: $\rho_k(z) = \rho_k(0)\ \exp(-mgz/T_k)$. The number density at the floor is determined by integrating $\rho_k(z)$ from $z = 0$ to ∞ and equalling this to N_k/L (i.e. the number of particles in the compartment divided by its width), which gives:

$$\rho_k(z) = \frac{mgN_k}{T_k L}\exp\left(-mgz/T_k\right). \qquad (6)$$

The value of $T_k\ [= \frac{1}{2}m\langle v_k^2\rangle$, from Equation (1) with $\langle v_{\mathrm{k}}\rangle = 0]$ is obtained from the energy balance (5) [21]:

$$T_k = \frac{m}{\pi}\left(\frac{afL}{\varepsilon N_k d}\right)^2, \qquad (7)$$

with d the particle diameter and $\varepsilon = (1-e^2)$ the inelasticity parameter. As expected, T_k increases if we increase the bottom velocity af, and decreases with growing number of particles N_k in the compartment.

This is a good point to say a few words about the dimensionless control parameters that govern the system. The traditional shaking parameter is the dimensionless shaking acceleration $\Gamma = a(2\pi f)^2/g$. However, in the present system the relevant combination of a and f must be af (i.e. the velocity of the vibrating bottom) rather than af^2. This is suggested by the expression for the temperature Equation (7), and can be understood from the non-dimensional form of the hydrodynamic equations. In particular, consider the combination of the equation of state (3) and the force balance (4):

$$\frac{\mathrm{d}(\rho T_{\mathrm{g}})}{\mathrm{d}z} = -mg\rho. \qquad (8)$$

This equation can be de-dimensionalised by replacing the height z by the non-dimensional height $\tilde{z} = z/h$, the number density ρ by the non-dimensional density $\tilde{\rho} = \rho/\rho_{\mathrm{cp}}$ (with ρ_{cp} the close-packed density, which in the 2D model corresponds to a hexagonal arrangement of the discs), and the temperature T_{g} by the non-dimensional temperature $\tilde{T}_g = T_{\mathrm{g}}/[m(af)^2]$

(with $m(af)^2$ being proportional to the energy imparted to the particles by the vibrating bottom). Equation (8) then takes the form

$$\frac{\mathrm{d}(\tilde{\rho}\tilde{T}_g)}{\mathrm{d}\tilde{z}} = -\frac{gh}{(af)^2}\tilde{\rho}, \tag{9}$$

from which we see that the dimensionless parameter $gh/(af)^2$ must play a key role in the present model. Other important dimensionless control parameters are the inelasticity ε and the filling factor $N_{\mathrm{tot}}d/KL$ (with N_{tot} the total number of particles in the system and K the number of compartments), which represents the overall particle content of the system. All these parameters can be recognised in the expression for the temperature Equation (7) and we will encounter them again in the next subsection.

3.2. *Flux model*

The particle flux from compartment k through the hole is proportional to $\rho_k(h)S(T_k/2\pi)^{1/2}$, i.e. the product of the number density at the height of the hole, the size of the hole S, and the velocity of the particles in the horizontal direction. This can be worked out to yield $F(\bar{N}_k) = F_0\bar{N}_k^2\exp\{-b\bar{N}_k^2\}$, where $\bar{N}_k$ denotes N_k/L (the number of particles in compartment k per unit width) and the factors F_0 and b are given by $F_0 = (2\pi)^{1/2}\varepsilon gSd/(af)$ and $b = \pi\varepsilon^2 ghd^2/(af)^2$ [21]. As anticipated, the particle flux is indeed a non-monotonic function of the number of particles in compartment k.

The flux function has also been measured directly in experiment and MD simulations, see e.g. [57,58]. The result is always a one-humped function, but where the theoretical Eggers function grows as $\bar{N}_k^2$ for small $\bar{N}_k$, the measured flux functions usually start out from $\bar{N}_k = 0$ with a power smaller than quadratic. This can be traced back to the fact that in Eggers' model the dissipation is taken to result from the binary collisions between the particles only (the frequency of which grows as $\bar{N}_k^2$), whereas in reality also the collisions of the particles with the walls (linear in $\bar{N}_k$) contribute. In the Knudsen limit $\bar{N}_k \to 0$ the particle–wall collisions even become the dominant source of dissipation. However, the most important feature of the flux function (its one-humped shape) is admirably captured by Eggers' model.

For our purposes, it will be convenient to write the flux as a function of the fraction $n_k = N_k/N_{\mathrm{tot}}$ contained in the kth compartment rather than as a function of N_k/L. The flux then takes the equivalent form [59]:

$$F(n_k) = An_k^2\exp(-\tilde{B}n_k^2), \tag{10}$$

where the fraction n_k is subject to the conservation condition $\sum_{k=1}^{2} n_k = 1$, and the factors A and $\tilde{B}$ take the form $A = (2\pi)^{1/2}\varepsilon gN_{\mathrm{tot}}^2 Sd/(afL^2)$ and $\tilde{B} = 4\pi\varepsilon^2[gh/(af)^2][N_{\mathrm{tot}}d/2L]^2$. This flux function $F(n_k)$ is depicted in Figure 6 for $A = 1\ \mathrm{s}^{-1}$ and $\tilde{B} = 6$.

The factor A determines the absolute rate of the flux. It must not be too large, in order to justify the assumption that the granular gas in each compartment separately is in a steady state, but its precise value is not important and may be incorporated in the time scale. The dimensionless parameter $\tilde{B}$ is of greater importance: its value determines whether the system will end up in the uniform state (for small $\tilde{B}$) or in the clustered state (for large $\tilde{B}$). Note that it combines the three dimensionless control parameters mentioned in the previous subsection all in one, namely the inelasticity ε, the shaking parameter $gh/(af)^2$, and the filling factor $N_{\mathrm{tot}}d/KL$. For a given setup and choice of beads (i.e. h, L, K, d and ε fixed) the value of $\tilde{B}$ can be raised either by increasing the total number of particles N_{tot}, or by *decreasing* the driving velocity af. In our experiments we usually use the latter option.

In order to make direct contact with our experiments we now replace the two-dimensional discs with the actual three-dimensional beads of Figure 2. The compartment width L is replaced by a compartment ground area Ω, and the aperture S between the compartments is no longer a 1D length but a 2D surface. This has no consequences for the general form of the flux function, which is still given by Equation (10), but the two factors A and $\tilde{B}$ now read:

$$A = c_1\frac{\varepsilon gN_{\mathrm{tot}}^2 Sd^2}{af\Omega^2}, \text{ and } \tilde{B} = c_2\varepsilon^2\frac{gh}{(af)^2}\left(\frac{N_{\mathrm{tot}}d^2}{\Omega}\right)^2 \equiv K^2B. \tag{11}$$

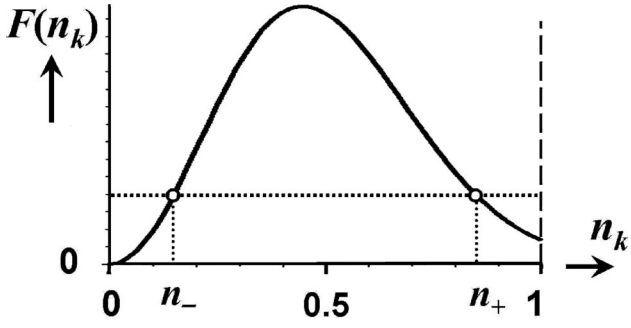

Figure 6. The flux function $F(n_k)$, i.e. the particle flux from compartment k as a function of the fraction n_k within that compartment. As a result of the inelasticity of the particle collisions, $F(n_k)$ only grows up to a certain value of n_k and decreases if the fraction is further increased. The horizontal dashed line shows that the flux from a relatively empty compartment (n_-) can be equal to the flux from a well-filled compartment (n_+), and this is exactly what happens in the clustered state. Note that the two fractions add up to one: $n_- + n_+ = 1$.

Here c_1 and c_2 are constants that we will use as free parameters to fix the timescale and the shaking parameter, respectively. Note that Equation (11) also introduces the alternative shaking parameter B ($= \tilde{B}/K^2$). This choice is sometimes preferable because the transition from the homogeneous configuration to the clustered state, which occurs at $\tilde{B} = K^2$, in terms of B always takes place at the same value $B = 1$, irrespective of the number of compartments K in the system. For the moment we proceed with the case of $K = 2$ compartments.

In the vigorous-shaking limit $\tilde{B} \to 0$ the exponential term in Equation (10) approaches unity, and in that case $F(n_k)$ grows monotonically with n_k, just as for an elastic gas with $\varepsilon = 0$. No balance between unequally filled compartments is possible in this case, and the system simply settles into the homogeneous state.

However, as $\tilde{B}$ is raised (by lowering the shaking strength) the exponential term comes into play, see Figure 6. The function $F(n_k)$ still starts out from zero at $n_k = 0$ and initially increases with n_k, but beyond $n_k = \tilde{B}^{-1/2}$ the function *decreases*, as a result of the dissipative effect of the increasingly frequent particle collisions. This enables a flux balance between a well-filled and a dilute compartment, provided the maximum of $F(n_k)$ lies at a value $n_k < \frac{1}{2}$ (i.e. $\tilde{B} > 4$). The condition $\sum n_k = 1$ can then be satisfied not only for an equal pair $n_1 = n_2 = \frac{1}{2}$ (corresponding to a flux level just beneath the maximum in Figure 6) but also for an unequal pair $n_1 \neq n_2$, corresponding to a smaller flux level indicated by the horizontal dashed line.

The dynamics of the system is governed by the following balance equation,

$$\frac{\mathrm{d}n_1}{\mathrm{d}t} = -F(n_1) + F(n_2) + \xi_1 = -F(n_1) + F(1 - n_1) + \xi_1, \qquad (12)$$

and analogously for $\mathrm{d}n_2/\mathrm{d}t$, which simply states that the time rate of change of the particle fraction in the kth compartment ($\mathrm{d}n_k/\mathrm{d}t$) is equal to the inflow from its neighbour minus the outflow from the compartment itself. The term ξ_1 is a Gaussian white noise term representing the fluctuations in the particle flux. As stated already in Section 1, granular gases are very suitable to study small-number statistical fluctuations, since they contain much less than the standard 10^{23} particles of textbook statistical systems. The influence of these fluctuations on the clustering transition was discussed by Eggers [21] and Lipowski and Droz [35], and worked out in detail by Mikkelsen et al. [58]. Corroborated by MD simulations, it was found that the system of Figure 2 is well described by the mean-field description of Equation (12), i.e. without the noise term, already for $N_{\mathrm{tot}} = 300$ particles. Only for smaller N_{tot} the statistical noise starts to dominate and the mean-field description breaks down [58]. In the present review, we will just assume that N_{tot} is sufficiently large to neglect the noise term, so we focus on the mean-field model only.

In equilibrium the time derivatives are zero, $\mathrm{d}n_k/\mathrm{d}t = 0$, and the two fluxes in Equation (12) must cancel each other [as foreseen in Equation (2)]: $F(n_1) = F(1-n_1)$. For $\tilde{B} < 4$ (or $B < 1$) this equality has only one solution: the symmetric state $n_1 = 0.5$. For $\tilde{B} \geq 4$ (or $B > 1$) this solution becomes unstable, but simultaneously two asymmetric stable solutions come into existence; one representing a state with a cluster in the left compartment, and the second one its (equivalent) mirror image with a cluster in the right compartment. The transition is depicted in Figure 7(*a*). The solid dots are experimental measurements at various values of B (each measurement consists of two points, n_1 and n_2, which together add up to 1) and the lines represent the equilibrium solutions of the flux model. Solid lines denote stable states and dashed lines unstable ones.

The clustering transition for $K = 2$ compartments is seen to be a pitchfork bifurcation, i.e. a second-order continuous phase transition. In accordance with this, the solid lines just beyond the critical point $B = 1$ are accurately described by $n_k = \frac{1}{2} \pm a(B-1)^{\beta}$, with critical exponent $\beta = 1/2$, which is the common (mean-field) power-law behaviour near a second-order phase transition [21,42,60].

4. Extension to more than two compartments

4.1. *Hysteretic clustering*

The Maxwell demon experiment is easily extended to more than two compartments. For a system consisting of K compartments in a row, or better still, in a ring such that the Kth and first compartment are neighbours,[9] the balance equation (12) takes the form:

$$\frac{\mathrm{d}n_k}{\mathrm{d}t} = F(n_{k-1}) - 2F(n_k) + F(n_{k+1}), \qquad (13)$$

with $k = 1,2, \ldots, K$ and $\sum_{k=1}^{K} n_k = 1$. We have disregarded the noise term ξ_k.

In contrast to the case for $K = 2$, the clustering transition for $K \geq 3$ is found to be abrupt and hysteretic, i.e. a first-order phase transition. Figure 7(*b*) shows the experimental results together with the flux model predictions for a cyclic three-compartment system [59]. The dots represent experimental runs that were started from the uniform distribution $\{\frac{1}{3}, \frac{1}{3}, \frac{1}{3}\}$, and the crosses represent experiments that were started from a single-peaked distribution ($\{1, 0, 0\}$ or one of its cyclic equivalents): we observe that there is an interval of B-values for which both the uniform and the clustered

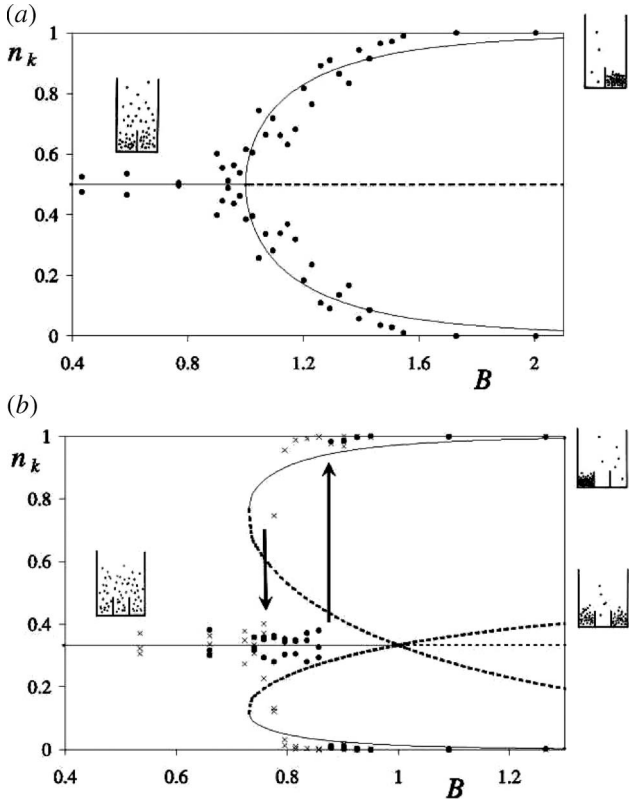

Figure 7. (*a*) Bifurcation diagram for the Maxwell demon experiment with $K = 2$ compartments ($k = 1, 2$). The dots are experimental data and the lines are the stable (solid) and unstable (dashed) equilibria predicted by the flux model of Equations (10) and (11). The transition to the clustered state is a continuous one, i.e. a second-order phase transition. (*b*) The same for $K = 3$ compartments ($k = 1, 2, 3$). The dots and crosses are experimental data: dots denote experimental runs that were started from the uniform distribution $\{\frac{1}{3}, \frac{1}{3}, \frac{1}{3}\}$ and crosses denote those that were started from a single peaked distribution. The transitions to and from the clustered state – indicated by the arrows – are abrupt and hysteretic, typical of a first-order phase transition (from [59]). Reprinted from Europhys Lett., 53, 328 (2001). Copyright 2001 by EDP Sciences.

state are stable. This is the region of hysteresis of the transition. If we start with a uniform distribution at strong shaking ($B \ll 1$) and slowly increase the value of B, the uniform state becomes unstable at $B = 1$. It is at this point that we get a clustered state. When B is then slowly turned down again, the clustered state remains stable until $B = 0.73$ and it is not before we reach this B-value that we witness the reverse transition to the uniform state.

The dashed curves for $B > 1$ that run above and below the horizontal line of the uniform distribution are associated with a transient state in which two of the compartments are competing for dominance, while the third compartment is already much more dilute. Starting out from the (unstable) uniform distribution, the system generally first goes through this transient state before it settles in the clustered equilibrium. No such transient states are encountered in the opposite transition for $B < 0.73$.

This hysteretic bifurcation diagram can be explained entirely by the flux model, which for three compartments takes the form:

$$\frac{\mathrm{d}n_1}{\mathrm{d}t} = -2F(n_1) + F(n_2) + F(n_3) = -2F(1 - n_2 - n_3) + F(n_2) + F(n_3), \quad (14)$$

and cyclic permutations for $\mathrm{d}n_2/\mathrm{d}t$ and $\mathrm{d}n_3/\mathrm{d}t$. All admissible distributions $\{n_1(t), n_2(t), n_3(t)\}$ (subject to the conservation condition $\sum_{k=1}^{3} n_k(t) = 1$) can be accommodated in a planar triangle, see Figure 8. The centre of this triangle represents the equal distribution $\{\frac{1}{3}, \frac{1}{3}, \frac{1}{3}\}$, while the corners correspond to $\{1, 0, 0\}$, $\{0, 1, 0\}$, and $\{0, 0, 1\}$, respectively.

The equilibrium solutions that are depicted in the bifurcation diagram Figure 7(*b*) are given by $\mathrm{d}n_k/\mathrm{d}t = 0$, $k = 1, 2, 3$. The uniform distribution $\{\frac{1}{3}, \frac{1}{3}, \frac{1}{3}\}$, which is an equilibrium for all B-values, is the most symmetric solution the system admits and when it becomes unstable (at $B = 1$) it gives way to solutions that necessarily have a lesser degree of symmetry. In the triangular plane these new solutions lie on the three lines of reduced symmetry $n_1 = n_2$, $n_1 = n_3$, or $n_2 = n_3$, see Figure 8. For example, the line $n_2 = n_3$ goes from the lower left corner $\{1, 0, 0\}$ to the middle of the right-hand side of the triangle, $\{0, \frac{1}{2}, \frac{1}{2}\}$. With $n_2 = n_3 \equiv n$, $n_1 = 1 - 2n$, and $\mathrm{d}n_2/\mathrm{d}t = \mathrm{d}n_3/\mathrm{d}t = -\frac{1}{2}\mathrm{d}n_1/\mathrm{d}t$, Equation (14) along this line takes the form:

$$\frac{\mathrm{d}n}{\mathrm{d}t} = F(1 - 2n) - F(n) = A\{(1 - 2n)^2 \exp[-9B(1 - 2n)^2] - n^2 \exp(-9Bn^2)\}, \quad (15)$$

and cyclic permutations along the other two (completely equivalent) symmetry lines. The situation is depicted in Figure 8 at four successive values of B.

At $B = 0.72$ (curve *a*) we see that $\mathrm{d}n/\mathrm{d}t$ has only one zero (steady state) on the relevant interval $0 \leq n \leq 1/2$, namely, at $n = 1/3$. This solution is stable, as one can easily check from the sign of $\mathrm{d}n/\mathrm{d}t$. So regardless of the initial condition the system always ends up in $\{\frac{1}{3}, \frac{1}{3}, \frac{1}{3}\}$: its basin of attraction (the shaded area in Figure 8) is the whole triangular plane. Next, for $B = B_{\mathrm{sn},3} = 0.73$ (not shown), the function $\mathrm{d}n/\mathrm{d}t$ touches zero at $n = 0.1255$, corresponding to a distribution $\{0.7490, 0.1255, 0.1255\}$ and its cyclic permutations. The index sn denotes that this involves a saddle-node bifurcation, while the index 3 stands for the number of compartments.

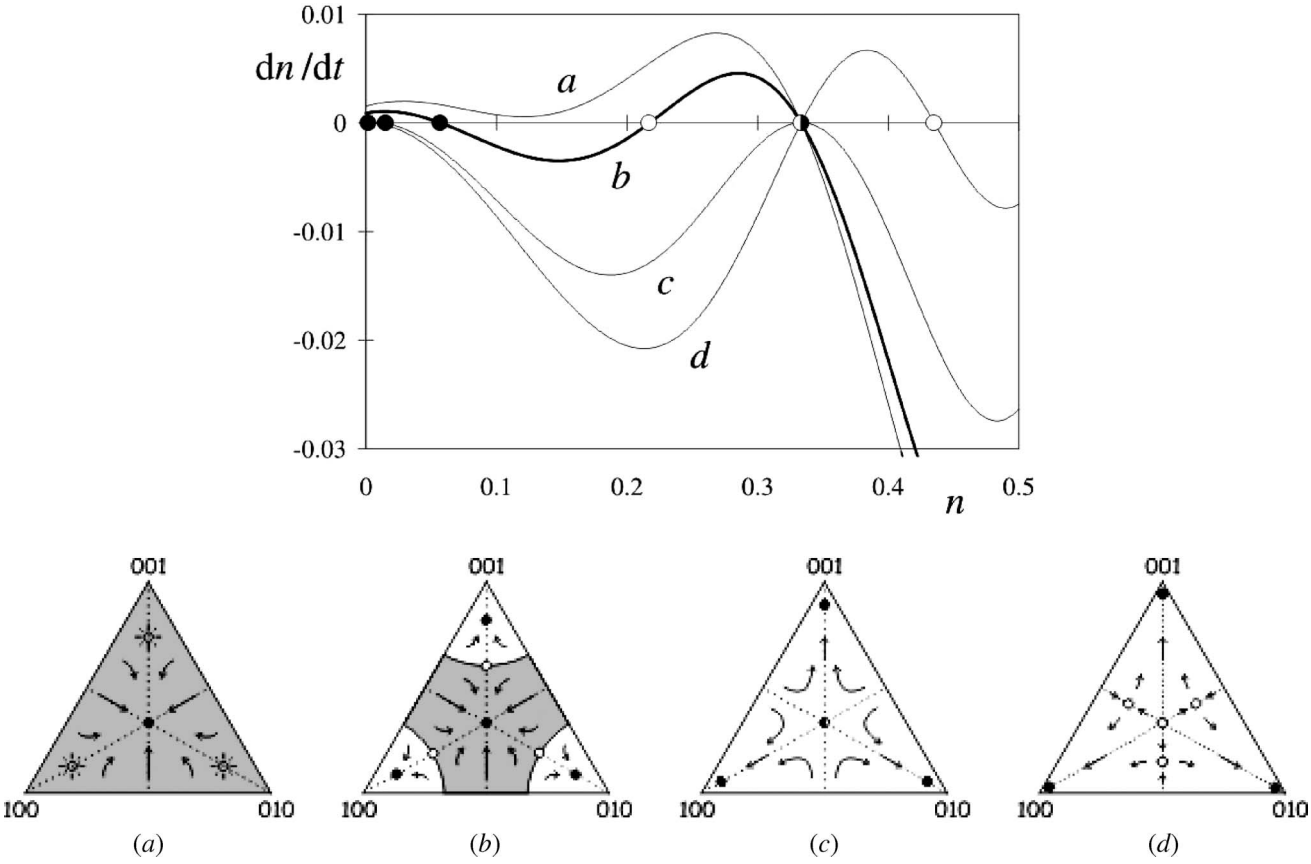

Figure 8. The rate of change dn/dt as function of n along the three symmetry axes of the three-compartment system (see Equation (15)), for four successive values of B: (*a*) $B = 0.72$, (*b*) $B = 0.78$, (*c*) $B = 1.0$, and (*d*) $B = 1.56$. For each of these values a triangular flow diagram is given, which shows the dynamics of the full system. The shaded area is the (diminishing) basin of attraction of the uniform equilibrium $\{\frac{1}{3}, \frac{1}{3}, \frac{1}{3}\}$ in the centre of the triangle; the white regions are the basins of attraction of the clustered solutions. Closed circles represent stable equilibria, open circles unstable ones. From [59]. Reprinted from Europhys Lett., 53, 328 (2001). Copyright 2001 by EDP Sciences.

In curve *b*, at $B = 0.78$, we see that dn/dt has meanwhile gone through zero, creating one stable and one unstable equilibrium along the line $n_2 = n_3$ (and, because of the threefold symmetry of the system, also along the lines $n_1 = n_2$ and $n_2 = n_3$). The three newly created *stable* equilibria are clustered distributions. Also the uniform distribution is still stable, so now there are four co-existing stable states, each one surrounded by its own basin of attraction. The three newly created *unstable* equilibria move towards the centre of the triangle, closing in upon $\{\frac{1}{3}, \frac{1}{3}, \frac{1}{3}\}$ and making its basin of attraction (the shaded area) smaller and smaller for increasing B.

Curve *c* depicts the situation for the critical value $B = 1.00$. The three unstable states have just reached the point $\{\frac{1}{3}, \frac{1}{3}, \frac{1}{3}\}$, reducing its basin of attraction to zero. At this instant the uniform distribution turns unstable. So from now on all initial configurations end up in one of the three clustered distributions.

Curve *d*, at $B = 1.56$, gives an impression of the final situation. The basins of attraction of the stable clustered states divide the triangle into three equal, kite-shaped parts. All the other equilibrium solutions (the three states that have gone through the point $\{\frac{1}{3}, \frac{1}{3}, \frac{1}{3}\}$, and the point $\{\frac{1}{3}, \frac{1}{3}, \frac{1}{3}\}$ itself) are unstable. The former are the transient states mentioned above, in which two of the compartments compete for dominance; they are saddle points, with stable branches along the symmetry lines (hence the negative slope of dn/dt in Figure 8) and unstable branches in the perpendicular directions, as indicated in the triangular plot. The symmetric solution $\{\frac{1}{3}, \frac{1}{3}, \frac{1}{3}\}$ is fully unstable.

The above sequence of events can be translated immediately into the bifurcation diagram of Figure 7(*b*). Moreover, it provides a physical reason for the hysteresis [59]: the forward transition at $B = 1$ has more degrees of freedom at its disposal than the reverse one at $B = B_{\mathrm{sn},3} = 0.73$. The former can take place via a variety of paths through any of the 2D kite-shaped sections of the flow diagram (see Figure 8(*d*)) whereas the latter is confined to take place along one of the 1D symmetry lines (see Figures 8(*a*) and (*b*)).

For the two-compartment system (where the analogous flow diagram reduces to a line) there is no room for any difference of freedom between the forward and backward transition, and hence there is no hysteresis.

As for the quantitative agreement between theory and experiment, we note that the experimentally measured ratio $B_{\text{reverse}}/B_{\text{forward}} \approx 0.88$ in Figure 7(*b*) is larger than the theoretical ratio 0.73. This can be attributed to statistical fluctuations in the particle fractions (which are typically of order $N_k^{-1/2}$, and larger near a bifurcation): close to $B = 1$ these fluctuations extend beyond the rapidly diminishing basin of attraction of $\{\frac{1}{3}, \frac{1}{3}, \frac{1}{3}\}$ and cause the system to switch prematurely to a clustered state, i.e. the forward transition for increasing B (see the dots in Figure 7(*b*)) occurs at a B-value that is smaller than $B_{\text{crit}} = 1$. Analogously, the reverse transition for decreasing B (see the crosses in Figure 7(*b*)) takes place at a value B_{reverse} that is somewhat larger than $B_{\text{sn},3} = 0.73$. Both effects conspire to make the experimentally measured ratio $B_{\text{reverse}}/B_{\text{forward}}$ larger than the theoretical prediction $B_{\text{sn},3}/B_{\text{crit}} = 0.73$. In addition, of course, one should recall that the Eggers flux function of Equation (10) is approximate, and that the theoretical prediction 0.73 is therefore an approximation, too. Any small changes in the function $F(n_k)$ will affect the ratio $B_{\text{sn},3}/B_{\text{crit}}$, however, not the qualitative properties of the model.

4.2. *Coarsening*

A first-order transition is found for all $K \geq 3$. The hysteretic behaviour becomes more pronounced when the number of compartments is increased, and the transient states become more numerous and also more important [61]. Figure 9(*a*) illustrates this for the case of $K = 5$ non-cyclic compartments. The region of hysteresis (where the uniform and the clustered state are both stable) now extends from $B = B_{\text{sn},5} = 0.34$ to $B = 1$ and the dashed lines of the transient states form a whole web, reaching even to the left of $B = 1$. They

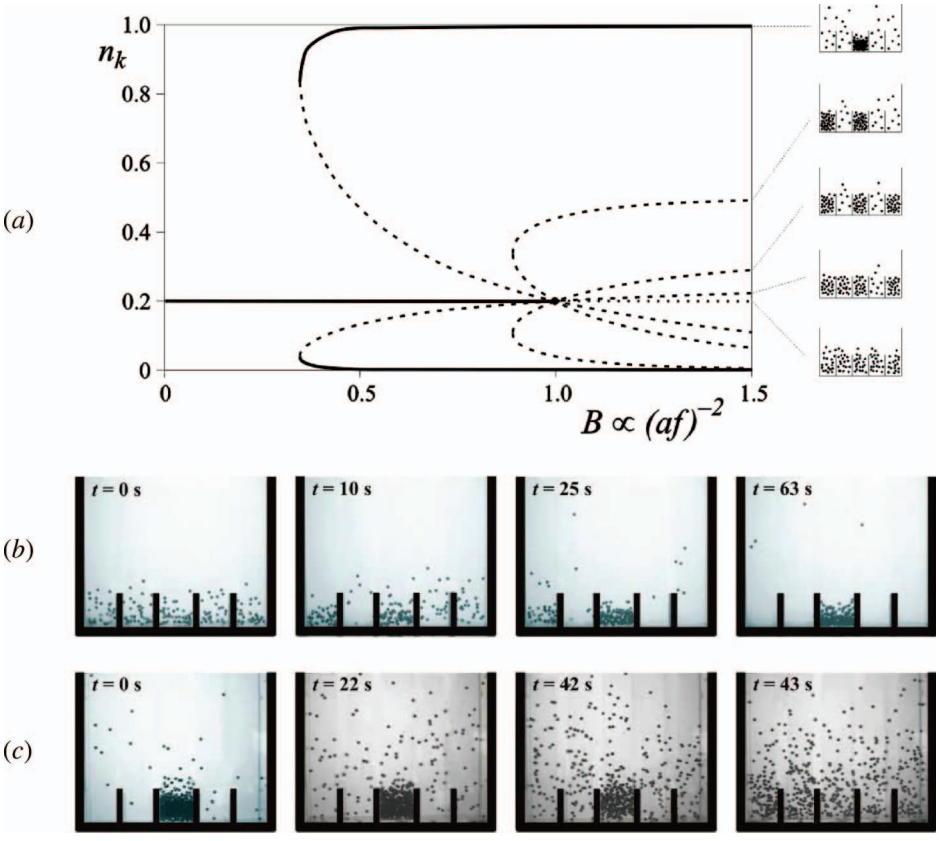

Figure 9. Maxwell demon experiment for $K = 5$ compartments. (*a*) Bifurcation diagram showing the stable (solid) and unstable (dashed) equilibria of the flux model. The sketches on the right depict the corresponding configurations. (*b*) Four stages in the clustering experiment at B slightly above 1, starting out from the (unstable) uniform state $n_k = 0.2$, $k = 1,...,5$. The particles do not cluster directly into one compartment but first go through a transient two-cluster state, which can be seen in the snapshots at $t = 10$ s and $t = 25$ s. (*c*) Breakdown of a cluster at stronger shaking ($B = 0.33$). The cluster is seen to survive up to $t = 42$ s, and then suddenly collapses: within one second the distribution becomes uniform (from [42]). K. van der Weele et al.: *The Physics of Granular Media*, H. Hinrichsen and D.E. Wolf, Editors. 2004. Copyright Wiley–VCH Verlag GmbH & Co. KGaA. Reproduced with permission.

correspond to states with $m = 2$, 3, 4 clusters, respectively, of which one representative configuration is depicted.

In Figure 9(b) four stages in the clustering process are shown for a B-value slightly above 1, starting out from the nearly uniform distribution. A two-cluster transient state is clearly visible at $t = 10$s and $t = 25$s, and it takes about a minute (i.e. 1260 vibration cycles) before the system gets past this state and reaches the one-cluster state. For larger values of K the experiment can easily get stuck in such a transient state (especially for low driving frequencies, i.e. $B \gg 1$) and it may take a very long time before the one-cluster state is reached, even though mathematically speaking this is the only truly stable equilibrium [61,62]. The clusters of the transient states collapse one by one, and the surviving clusters get larger, in an exceptionally slow coarsening process: whereas the characteristic sizes in most coarsening processes in nature grow as $t^{1/2}$ (or some similar algebraic rate), the size of the surviving granular clusters is found to increase only at the snail's pace of $[\log(t)]^{1/2}$ [63–65].

The opposite process of *declustering*, depicted in Figure 9(c) for a B-value just below $B_{\mathrm{sn},5}$, is also of interest. Not only because declustering is more desirable in practical applications (e.g. in sorting machines and conveyor belts, where clustering is definitely an unwanted phenomenon) but also because the breakdown of a cluster turns out to be by no means the same as clustering in reverse time order. This in itself is not surprising, since a certain lack of time-reversal symmetry is to be expected in any dissipative system, but it is the degree to which the symmetry is broken which makes it spectacular here. Van der Meer et al. [66] discovered that the breakdown takes place via a 'sudden collapse': starting out with all particles in one compartment, the cluster seems stable for a considerable time, spilling only a small number of particles to its neighbours. However, at a certain moment (between $t = 42$ and 43 s in the experiment of Figure 9(c)) the cluster suddenly collapses and the particles spread out over all compartments. This collapse, which can be delayed for extremely long times if B approaches the critical value $B_{\mathrm{sn},K}$ (with the cluster lifetime diverging as $[B_{\mathrm{sn},K} - B]^{-1/2}$) has been studied in detail in [66] and [67].

5. How the demon can be put to work

5.1. Granular fountain

In this section we will see how the demon can be turned into a helpful creature and be made to extract useful work from the stochastically moving particles. To this end we add a new element to the two-compartment system: a small hole in the wall, located at the bottom (see Figure 10), thereby allowing also the less energetic particles to switch compartment. This seemingly small modification turns out to have a major influence on the behaviour of the system.

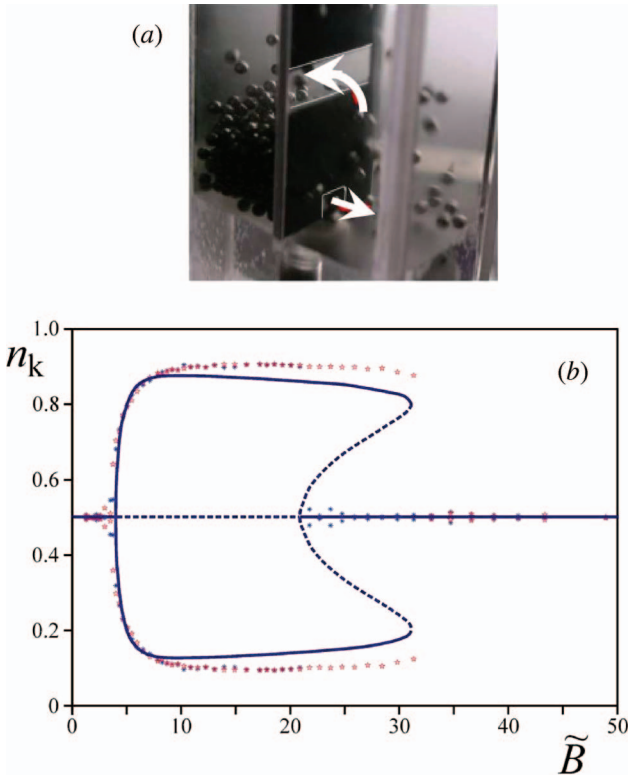

Figure 10. The granular fountain: (a) the experiment, with arrows indicating the direction of the particle flux through the two openings. The flux through the opening at height h is directed towards the dense compartment, whereas the flux through the small hole is directed towards the dilute compartment. (b) The corresponding bifurcation diagram, showing the flux model predictions (solid curves for stable states, dashed for unstable ones) together with the experimental measurements. The shaking parameter along the horizontal axis is $\tilde{B} = \underline{K}^2\underline{B} = 4\underline{B}$. The blue asterisks represent experiments that were started from the symmetric initial condition $\{\frac{1}{2}, \frac{1}{2}\}$; the red stars those that were started from an initial state with all particles in one compartment, i.e. either $\{1, 0\}$ or $\{0, 1\}$.

The density difference between the dense and dilute compartment induces a flow through the hole towards the latter. When a particle enters the diluted compartment, it soon picks up sufficient kinetic energy from the vibrating bottom to jump over the wall again, leading to a stable convection roll as shown in Figure 10(a). The collective motion of the particles is *upwards* in the hot (dilute) compartment and *downwards* in the cold (dense) one. This is called the granular fountain [68].

In terms of the flux model, the hole introduces an extra term in the flux function:

$$F_{\mathrm{fount}}(n_k) = F(n_k) + \lambda F_0(n_k) = An_k^2 \exp(-\tilde{B}n_k^2) + \lambda An_k^2. \tag{16}$$

The flux-through-the-hole $\lambda F_0(n_k)$ is in principle of the same form as the flux over the wall, but since the hole is located at zero height (hence the subscript 0) the corresponding value of $\tilde{B}$ is zero and the exponential part is suppressed. The prefactor λ is determined by the size of the hole. Evidently, this size must be at least as large as a particle diameter to have any effect. On the other hand it should not be made too large, otherwise the flux through the hole will be too abundant and always establish a uniform equilibrium between the compartments.

In Figure 10(*b*) we show the bifurcation diagram determined by the flux model (solid and dashed lines) and experimental measurements (indicated by the asterisks and stars). We see that the transition from the uniform distribution to the fountain state (upon increasing B) occurs through a pitchfork bifurcation just as for the original two-compartment system. The fountain state is stable in the interval $1 \leq B \leq 8.2$, or equivalently $4 \leq \tilde{B} \leq 32.8$ (with $\tilde{B} = K^2 B = 4B$, cf. Equation (11)). When B is increased further, it breaks down and gives way to the uniform state again, this time via a discontinuous, first-order phase transition [68,69]. In this high-B regime, the shaking is so weak that the particles do not get sufficient kinetic energy anymore to jump to height h (not even in a diluted compartment) and the only active opening is the hole at the bottom, via which a uniform equilibrium is established.

Just like the original Maxwell demon system, the two-compartment fountain can be extended to $K \geq 3$ compartments [65,69]. In that case, for increasing B (decreasing shaking strength) one finds a stepwise transition from the uniform state with K hot compartments, first to a one-cluster state (1 cold compartment and $K-1$ hot ones), then to a two-cluster state (2 cold compartments and $K-2$ hot ones), and so on, until at some low shaking strength one arrives at the situation with K cold compartments (and zero hot ones), which is simply a uniform state again. For $K \geq 3$ all the successive steps in this cascade, including the first one at $B = 1$, are hysteretic first-order transitions.

5.2. *A granular Brownian motor*

We now go one step further: we take a cyclic K-compartment system (with K even) and alternatingly close the lower and the upper passage in the walls. As is seen in Figure 11(*a*), the separate convection rolls now join together into one continuous collective motion that meanders sideways through the entire system. That is, the convective motion between adjacent compartments has been translated into a directed motion along the whole length of the system. This is a Brownian motor, i.e. a system in which isotropic noise (from the stochastically colliding particles) is converted into a directed motion [68,70–72]. It is in fact a very special type of Brownian motor, since the directed motion does not arise from any geometric asymmetry in the setup but from the spontaneous symmetry breaking induced by the clustering effect. This means that, starting from a uniform particle distribution, the meandering motion may be excited equally well in the opposite direction.

In the flux model, we now alternatingly have only the first term $F(n_k)$ or the second term $\lambda F_0(n_k)$ of the fountain flux function (cf. Equation (16)):

$$\frac{\mathrm{d}n_k}{\mathrm{d}t} = \lambda F_0(n_{k-1}) - \lambda F_0(n_k) - F(n_k) + F(n_{k+1}), \quad (17)$$

$$\frac{\mathrm{d}n_{k+1}}{\mathrm{d}t} = F(n_k) - F(n_{k+1}) - \lambda F_0(n_{k+1}) + \lambda F_0(n_{k+2}), \quad (18)$$

where the first equation represents the compartments with a lower passage at their left-hand side, and the second equation the adjacent ones, which have an upper passage at the left-hand side. Figure 11(*b*) shows the bifurcation diagram for the smallest conceivable motor, namely for $K = 4$.[10] It features co-existing non-symmetric states of two different types:

(1) *Ratchet states* with alternating dense and dilute compartments and a net particle flux through the system (black solid curves in Figure 11(*b*)). The non-zero value of this flux is the hallmark of a spontaneous ratchet effect, i.e. the Brownian motor. Obviously the magnitude of the net flux will be exactly the same as that of the convective flow in the corresponding granular fountain.
(2) *Fluxless clustered states* consisting of K dense and K dilute compartments, but not in the order dense–dilute–dense–dilute needed for the directed motion (red solid curves in Figure 11(*b*)), which means that there is *no* net particle flux, but simply a local dynamical balance between adjacent compartments. The clustering is somewhat more pronounced than in the ratchet state. The reason for this is that in the ratchet state (due to the positive net flux) there are always a few extra particles in the dilute compartments, just passing by on their way to the next dense compartment.

Starting from the uniform distribution at vigorous driving (i.e. low B), at $B = 1$ or $\tilde{B} = 16$, with $\tilde{B} = K^2 B = 16B$, a fluxless clustered state comes into existence through a pitchfork bifurcation, rendering the uniform state unstable with respect to perturbations in the directions $\{+--+\}$ and (equivalently)

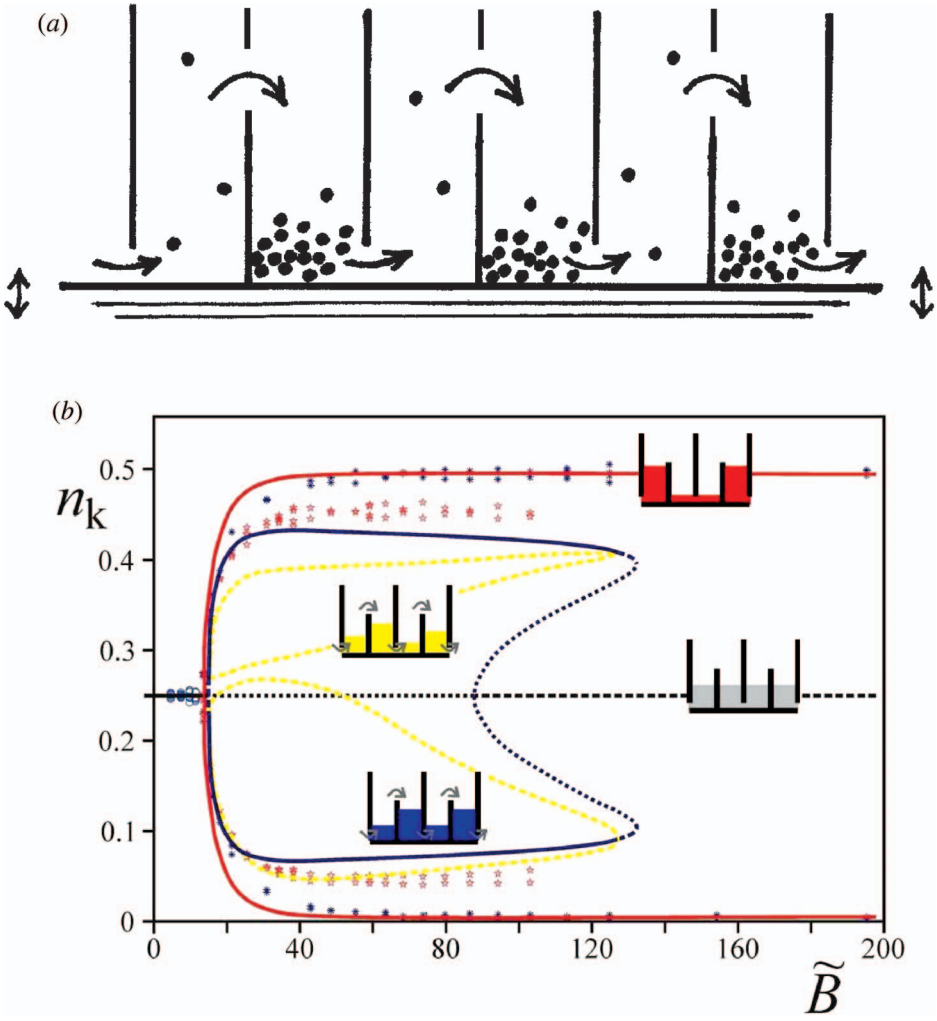

Figure 11. A granular Brownian motor: (*a*) sketch of the setup, where the boundary conditions are understood to be cyclic. Just as in the fountain (Figure 10) the net flux through the slits at height h is directed towards the dense compartments, and the flux through the holes at the bottom is directed towards the dilute compartments. This sustains a directed motion throughout the system, called the ratchet effect. (*b*) The corresponding bifurcation diagram for $K = 4$ compartments and $\lambda = 0.05$ (cf. Equation (16)). The shaking parameter along the horizontal axis is $\tilde{B} = K^2 B = 16B$. At $B = 1$ the uniform distribution $n_k = 0.25$ ($k = 1, \ldots, 4$) becomes unstable, giving way to a stable fluxless clustered state through a pitchfork bifurcation (red curves). A second pitchfork bifurcation (at $B \approx 1.2$) generates the ratchet state, with a non-zero net flux (blue curves). The ratchet state is stabilised through a third pitchfork bifurcation at $B \approx 1.25$ (in which a completely asymmetric, unstable state is created, indicated by the yellow curves) and destabilises again at $B \approx 3.8$ when it recombines with this same asymmetric state. Solid lines correspond to stable solutions, dashed and dotted lines to unstable ones.

$\{-++-\}$. Soon afterwards, at $B \approx 1.2$, the uniform state becomes unstable also to perturbations in the directions $\{+-+-\}$ and $\{-+-+\}$, through a second pitchfork bifurcation, and the ratchet state comes into existence. At birth, this ratchet state is still unstable, but it is soon stabilised by the generation of an unstable asymmetric state in which all four compartments have a different fraction n_k. Now follows an interval in which the ratchet state and the fluxless clustered state are both stable, until at $B \approx 3.8$ the ratchet state and the completely asymmetric state recombine into an unstable ratchet state, which eventually disappears through a saddle-node bifurcation at $B \approx 4.1$. From $B \approx 3.8$ on, the fluxless clustered state is the only stable state in the system.

The ratchet effect is possible for all even-numbered $K \geq 4$, but the chances that the required strict alternation of dense and dilute compartments $\{..+-+-..\}$ arises spontaneously from a uniform state swiftly decrease for growing K. Any deviation from this pattern will block the net flux. Of course, it always remains possible to induce the ratchet effect by means of a properly chosen initial particle distribution, or by applying a small external force (during a certain preparatory time span) in the horizontal direction in Figure 11(*a*). This is comparable to other systems with

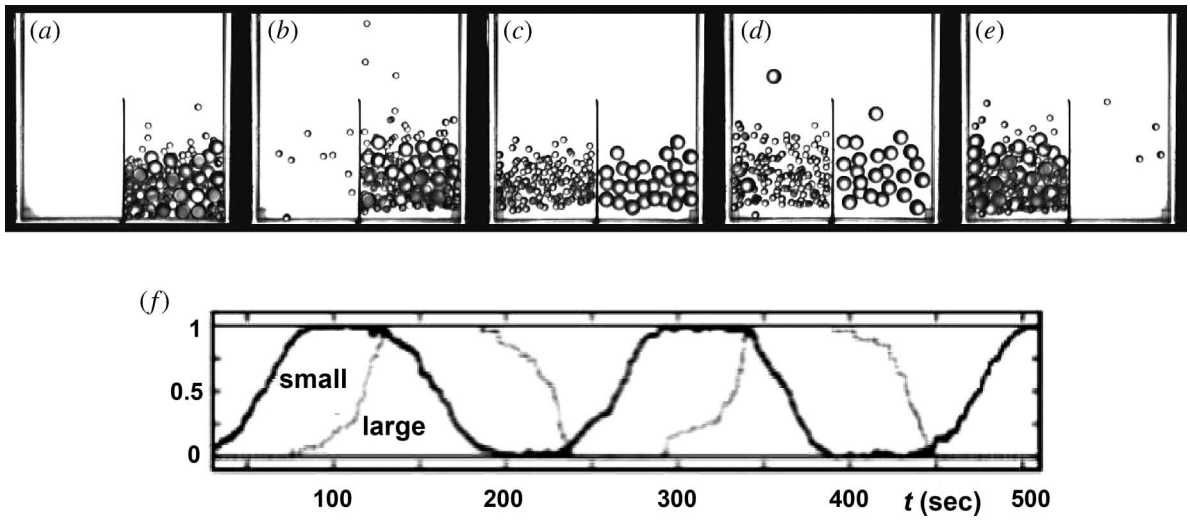

Figure 12. Granular clock: (*a*)–(*e*) a mixture of 27 large glass beads (diameter 4 mm) and 138 small ones (diameter 2 mm) shaken at $f = 20$ Hz and $a = 6$ mm; shaking parameter $af = 0.12$ ms^{-1}. The five snapshots, taken at $t = 237$, 240, 295, 303 and 340 s, cover one-half of the clock's period. (*f*) The experimentally measured particle fractions in the left compartment as a function of time. The cluster oscillates back and forth between the left and right compartment with period 206 s. From [77]. Reprinted figure with permission from S. Viridi, M. Schmick, and M. Markus, Phys. Rev. E., 74, 041301, 2006. Copyright (2006) by the American Physical Society.

spontaneous symmetry breaking, e.g. a ferromagnet:[11] just like a piece of iron picked from the shelf normally appears to be unmagnetised and an external magnetic field is needed to produce a magnetisation on a global scale, a ratchet state for large K needs some initial bias.

6. Particles of different size

6.1. Granular clock

Up to now we have been considering granular gases that consisted of identical spherical particles, but in practice most granular systems are not quite like that. Usually there is some spread in the size, form, and density of the particles. In that case the clustering can take even more interesting forms than before [73,74]. Here we consider a mixture of large and small beads (i.e. spherical particles of two sizes, which in every other respect are equal): this is the setting for a remarkable effect called the *granular clock*, in which the cluster switches periodically from one compartment to the other [75–78]. The same phenomenon also occurs in mixtures of beads that have the same size but different density [33,79].

The granular clock effect, first predicted on the basis of numerical simulations [75] and theory [76], was demonstrated experimentally by Viridi et al. [77,78] (see Figure 12). The setup consists of two compartments, just as in the original Maxwell demon experiment, but now with 27 large glass beads (diameter $d_L = 4$ mm) and 138 smaller ones ($d_S = 2$ mm). Initially all the beads are positioned in the right compartment. At vigorous shaking ($af > 0.17$ ms^{-1}), the beads – large and small – spread out evenly over the two compartments. And if the shaking is too weak ($af < 0.08$ m s^{-1}), the particles are unable to jump over the wall and remain in the right compartment forever. This is all just as in the monodisperse case.

It is for intermediate shaking strengths that the interesting new effects come into play. The large particles stay close to the bottom, forming a kind of mattress for the smaller ones. Thanks to this mattress, the small beads jump higher than they would on the plain floor, not just because the large ones occupy the layer close to the floor and thereby drive the smaller ones to the higher regions but mainly because of the favourable momentum transfer from the large to the small beads, by which the latter (due to their small mass) gain high velocities. The situation is reminiscent of the demonstration experiment in which one puts a tennis ball on top of a basketball and let them drop together: upon hitting the ground, the tennis ball is literally launched into the air, flying much higher than its release height [80].

First, if the shaking is made strong enough to let one small bead jump over the wall ($af > 0.08$ ms^{-1}), all the small ones will follow, since with every bead that leaves the compartment the remaining ones lose less energy in collisions and thus become more energetic. For $0.08 < af < 0.11$ ms^{-1} the large particles are not mobile enough to follow suit and thus we get a perfect separation of small and large beads: the large ones are still in the right compartment and all the small ones now reside in the left compartment. Without a mattress they are unable to jump back into the right compartment, so the separated state is stable. In fact, for the

particle numbers chosen in this experiment (only 27 large ones against 138 small ones) the large ones now actually jump slightly higher than the small ones.

When af is increased beyond 0.11 m s^{-1}, we get the situation of Figure 12(*a*)–(*e*). Now the large particles *are* able to follow the smaller ones over the wall. This exodus speeds up with every bead that leaves the compartment, and before long all – or practically all – particles are in the left compartment (Figure 12(*e*)). But this is just the initial state in mirror image! So the whole process will start all over again in the opposite direction, and will in fact repeat itself indefinitely, with the cluster going back and forth periodically between the two compartments. This is the granular clock effect.

Figure 12(*f*) shows the experimentally measured fractions in the left compartment for $a = 6$ mm and $f = 20$ Hz (i.e. $af = 0.12$ ms^{-1}). One sees clearly how the small beads (solid curve) precede the large ones (dashed curve) and that, as soon as the switch from right to left compartment is complete, the reverse process towards the right compartment sets in without delay. The period of oscillation in this case is 206 s.

The clock effect in this experiment was found to be stable for $0.11 \leq af \leq 0.17$ ms^{-1}, and its period in this interval was observed to decrease steadily from 10 min at $af = 0.11$ ms^{-1} to roughly 1 min at $af = 0.17$ ms^{-1}. Close to this latter threshold value the separation becomes less and less perfect (the compartments are never entirely diluted anymore) and for $af > 0.17$ ms^{-1} the beads just spread out uniformly over the two compartments. Mathematically, this transition from the periodic behaviour of the clock state to the steady uniform distribution is a reverse Hopf bifurcation [33].

Just as the clustering phenomena of the previous sections, also the granular clock effect can be described (qualitatively and quantitatively) by the flux model, provided that it is modified to account for the fact that we now have two particle species, small and large, which influence each other in a non-trivial way. Various bidisperse flux functions have been proposed in the literature [33,73,75,76,78,82]. The granular clock is described particularly well by the phenomenological models of [78] and [33].

6.2. *David versus Goliath*

The granular clock effect is not the only interesting feature of bidisperse particle mixtures. As a second example, in Figure 13 we show the phenomenon of *competitive clustering* known as the David-versus-Goliath effect [73,81,82]. We will keep the description at a qualitative level, but also this effect admits a quantitative treatment in terms of a bidisperse version of the flux model [73,82].

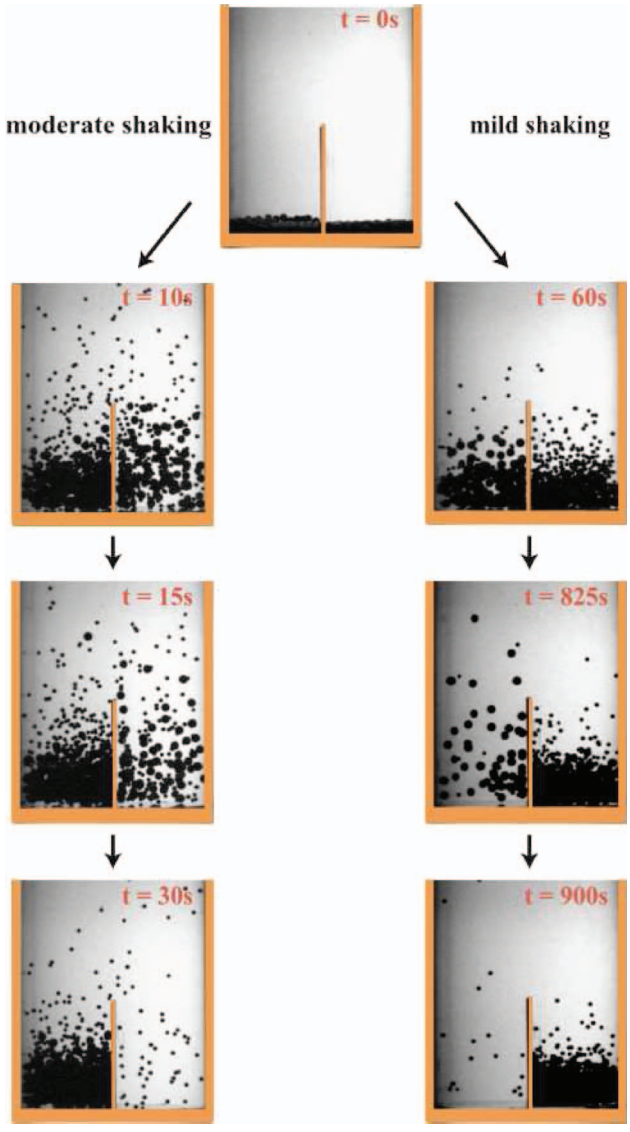

Figure 13. The David-versus-Goliath effect: competitive clustering in a bidisperse mixture of large and small beads. The initial condition (topmost picture) has {180 large, 200 small} in the left compartment and {120 large, 400 small} in the right one, meaning that 55% of the total particle mass is initially in the left compartment. For relatively strong shaking (left column, $f = 60.0$ Hz and $a = 1$ mm) the cluster is formed in the left compartment: Goliath wins. For mild shaking (right column, $f = 37.5$ Hz and $a = 1$ mm) it goes into the right compartment: David wins. For very strong shaking (not shown) the particles spread evenly over the two compartments, whereas for very weak shaking the particles are unable to jump over the wall and the initial distribution remains intact. From [82]. Reprinted figure with permission from R. Mikkelsen et al., Phys. Rev. E, 70, 061307, 2004. Copyright (2004) by the American Physical Society.

The setup this time contains 300 large steel beads (diameter $d_L = 5.0$ mm) and 600 smaller ones ($d_S = 2.5$ mm), and in the initial state we have {180 large, 200 small} in the left compartment, and hence {120 large,

400 small} in the right compartment. This means that initially 55% of the total particle mass is in the left compartment.

Starting out from this initial condition at shaking parameters $f = 60$ Hz and $a = 1$ mm (i.e. $af = 0.60$ ms^{-1}), the beads cluster together in the left compartment, see Figure 13 left column. This is what one would expect, since the larger particle mass in the left compartment gives this compartment a head start. It takes about half a minute for the cluster to develop.

If we decrease the shaking below a critical threshold, however, the same initial condition now leads to a cluster in the *right* compartment! This is illustrated in Figure 13 right column, for $f = 37.5$ Hz and $a = 1$ mm (i.e. $af = 0.375$ ms^{-1}). The series of events is similar to what we saw in the granular clock: at first the large particles stay close to the floor, transferring energy from the vibrating bottom to the smaller ones above them, which thereby gain relatively high velocities. The effect is stronger in the left box – which has more large particles – than in the right box, and thus the small beads go preferentially into the latter. As a consequence, the remaining particles in the left compartment become more mobile as well and begin to make it over the wall into the right compartment, where they are immediately swallowed by the developing cluster. With every large particle that leaves the left compartment, the process progressively speeds up and (in the experiment of Figure 13, right column) the clustering is complete after 15 min.

So, simply by tuning the shaking strength, the clustering can be directed. This opens up new possibilities for the handling and processing of bidisperse granular materials in practical applications.

7. Conclusion

7.1. Summary, and a new beginning

In conclusion, we have seen that Maxwell's demon rules in granular gases. The flux model, based on granular hydrodynamics, provides a quantitative description of the clustering phenomenon not only in the original two-compartment system, but also in the various extended systems that we have discussed. For more than two compartments the clustering was seen to take place via a series of transient states in which the various compartments competed for dominance. Via a slight adaptation in the setup (an extra hole in the wall between the compartments) we were able to make the demon *work* for us, in the form of a granular fountain and also in the form of a Brownian motor. Finally, by introducing particles of different size into the system, the demon was seen to give rise to the granular clock and to the competitive clustering phenomenon known as the David-versus-Goliath effect.

It will be clear that the generalisations and applications of the Maxwell demon experiment are by no means exhausted yet, especially when one realises that these need not be restricted to granular gases. The same ideas may be applied to any many-particle system out of thermodynamic equilibrium. A point in case is the formation of sand ripples along the beach, which is well described by a similar flux model [83]. An even more striking example – from an entirely different field – concerns the formation of traffic jams, i.e. the clustering of *cars*. We will briefly discuss it here to underline the ubiquity of Maxwell's demon in non-equilibrium systems.

7.2. Maxwell's Demon on the highway

Even though at first sight they may seem quite unrelated, cars on the highway resemble in many ways a one-dimensional, unidirectional granular gas. The analogy is in fact so strong that it has led to a series of bi-annual conferences 'Traffic and Granular Flow' [84]. The engines provide the necessary energy input (the cars are self-driven particles) and just as the particles in a granular gas, the cars interact inelastically. They do so without actual collisions, but simply because a car that closes in upon another must reduce its speed, as illustrated in Figure 14(*a*). A tiny flaw in the analogy is that momentum is not conserved here[12] but the fact remains that cars, just like particles, make each other slow and traffic jams are the natural result [85,86].

The mean velocity v of the cars is a decreasing function of their density ρ, as can be seen from the experimental data in Figure 14(*b*), measured on the highway A58 in the Netherlands, at a specific point close to the city of Eindhoven. At low density, up to $\rho_k \approx 30$ veh km^{-1} lane^{-1}, the cars drive at their desired velocity of roughly 110 km h^{-1} (with quite a large spread, partly due to the fact that the data include both passenger cars and trucks). Above 30 veh km^{-1} lane^{-1} the distance between successive cars becomes so small (less than 30 m) that the drivers can no longer maintain this desired velocity. They have to react, brake, and manoeuvre, and this causes a sudden drop in the velocity.

The corresponding car flux across the measuring point (density ρ times velocity v), also known as the 'fundamental traffic diagram' [85–87], is shown in Figure 14(*c*). It shows the two regimes even more clearly than the velocity itself: at low densities the cars flow freely, and the flux function $F(\rho_k)$ shows an upward branch rising to nearly 3000 veh h^{-1} lane^{-1} at $\rho_k = 30$ veh km^{-1} lane^{-1}. Above 30 veh km^{-1} lane^{-1} the traffic becomes congested, and the flux goes down dramatically. Just like the granular flux function of Figure 6, the car flux $F(\rho_k)$ depends in a non-monotonic way on the density, which – as we have seen – is a

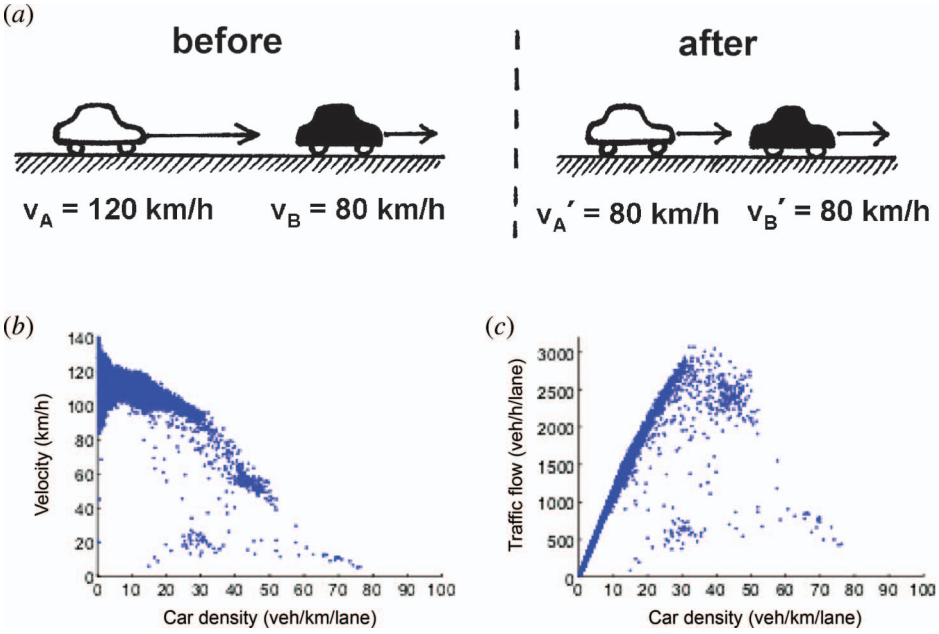

Figure 14. Maxwell's demon on the highway: (*a*) inelastic interaction of two cars. The white car has to adjust its speed to that of the black car in front of it: $\{v_A, v_B\} \to \{v'_A, v'_B\} = \{v_B, v_B\}$. (*b*) Speed of the traffic passing a certain monitoring point (k) on the highway A58 in the Netherlands versus the local car density ρ_k. Each point is a 5 min average of measurements of the morning traffic collected during 15 working days without accidents or exceptional weather conditions in the autumn of 2001. (*c*) The corresponding car flux (=density times speed), also known as the fundamental traffic diagram. Note the similarity with the particle flux function in Figure 6 (from [86]). Figures (*b*) and (*c*) reprinted with permission from Hoogendoorn et al., *Traffic and Granular Flow '03*, Springer, Berlin, 2005.

crucial prerequisite for clustering. However, the data in the (F,ρ)-plane do not follow a one-dimensional function but are scattered over a two-dimensional area, corresponding to various types of congested traffic (synchronised flow, jams, etc. [88,89]). In this case we therefore get a better correspondence if we work with a two-dimensional flux function $F(\rho_k,\rho_{k+1})$, i.e. if we let it depend not only on the density at the location k but also on that at the target location $k+1$ (roughly 1 km ahead). This expresses the fact that drivers react on the situation ahead of them. The flux model for traffic then takes the following form:

$$\frac{\mathrm{d}\rho_k(t)}{\mathrm{d}t} = \frac{1}{\Delta x}\{F(\rho_{k-1},\rho_k) - F(\rho_k,\rho_{k+1})\} + Q_k(t), \tag{19}$$

where $\Delta x = 1$ km is the distance between successive measuring points and the term $Q_k(t)$ represents the inflow and outflow of cars at junctions and ramps. This term (which is non-zero only at certain locations k) expresses a special feature of the traffic jam problem, namely that the number of cars is not conserved.

Like the original Maxwell demon experiment, also the traffic model can be extended to incorporate cars of different size (differentiating between passenger cars and trucks makes the model bidisperse) or to work with different forms of the flux function at different points k (since the road is not everywhere the same, due to e.g. construction works, dangerous bends, or intersections). But even the simple version of Equation (14) has been proven able to reconstruct, and even predict, traffic jam formation on the highway A58 in the Netherlands [86]. It also correctly describes the backward group velocity of 18 km h^{-1}, one of the most robust characteristics of traffic jams observed on all highways around the world.[13] In other words, Maxwell's Demon rules on the highway just as it does in granular gases.

Acknowledgements

I am grateful to Jens Eggers, Isaac Goldhirsch, and Mario Markus for kindly permitting me to reproduce their figures, and for their positive and extremely valuable feedback on an early draft of the paper. Many thanks are also due to the referees for their anonymous help in improving the paper via a series of wonderfully insightful comments. Finally, I want to thank Devaraj van der Meer and Detlef Lohse, with whom I had the pleasure to work together on many fascinating aspects of Maxwell's demon in granular gases.

Notes

1. Due to the redirected forces, the pressure on the side walls can become uncomfortably high. In the United States alone some 1000 grain silos collapse every year due to overpressure on the side walls.

2. The dimensionless number that measures the influence of the ambient medium is the Bagnold number Ba, defined as the ratio between a typical Newtonian force acting on the particle (gravity, friction, collisions) and the most relevant force from the medium (drag, lift). A good choice in many cases is to take the gravitational force and the Stokes drag force: $\mathrm{Ba} = mg/3\pi\eta dv = \rho_s d^2 g/18\eta v$, where η is the dynamic viscosity of the medium, d and ρ_s are the diameter and material density of the particles, and v is their characteristic velocity. For $\mathrm{Ba} \gg 1$ the influence of the medium may be neglected; when Ba becomes of the order of 1 or smaller the surrounding medium must be taken into account. For the systems discussed in the present review, with glass beads ($\rho_s = 2.5\ 10^3$ kg m^{-3}) of diameter $d = 2\ 10^{-3}$ m and typical velocity $v = 1$ ms^{-1}, moving through air at room temperature and atmospheric pressure ($\eta = 1.8 \times 10^{-5}$ kg/sm), the value of the Bagnold number is roughly 300.
3. Barchans are crescent-shaped dunes that form in desert areas with a firm underground and a limited sand supply where the wind blows in one prevailing direction. They propagate in the direction of the wind at a typical velocity of several tens of metres per year, with smaller dunes moving faster than big ones and occasionally overtaking them. For an introduction to the extensive literature on barchan dunes we refer to [16]. Also recommended are the beautiful photographs by NASA of the barchan fields on Mars, see e.g. [17].
4. An additional and slightly deeper reason for the prominence of fluctuations is the fact that granular matter has weak scale separation (or no separation at all) between the microscopic and macroscopic scales, see e.g. [20].
5. Since the setup is symmetric, it is a matter of chance which of the two compartments will be preferred.
6. The analogy with thermodynamic temperature should be handled with care, since the ensemble averages implied in Equation (1) may not directly apply to single realisations [20,30] and – if the system contains non-identical particles – the lack of energy equipartition between the various species may be a complicating factor, with different species having different granular temperatures [31–33].
7. Recent experiments suggest that this identification ($T_g = \frac{1}{2}m\langle v^2\rangle$) holds quite generally for vibrated granular gases of identical particles, and that (except for the bottom layer) the velocity distribution is very nearly Maxwellian throughout the system, see [34].
8. In this situation, the mean free path length ℓ of the particles is of the same order as the system size and the gas is called a Knudsen gas. If the dimensionless Knudsen number Kn (defined as the ratio of the mean free path to the system size) is of the order of 1 or higher, the continuum assumption underlying fluid mechanics is no longer a good approximation and statistical methods should be used instead.
9. A non-cyclic array is described by the same Equation (13), only modified at the end compartments $k = 1$ and $k = K$. The results do not differ significantly from those for a cyclic array [61].
10. Note that for $K = 2$ the Brownian motor setup is simply equivalent to the granular fountain of Figure 10.
11. For the analogy, the compartments of the ratchet system should be compared pairwise (a cluster and an adjacent dilute compartment) to the individual magnetic domains in the piece of ferromagnetic material.
12. The interactions in a granular gas conserve mass and momentum (but not energy), whereas in traffic only mass is conserved. This is a source of difference between granular and traffic flow – and obviously it is not the only one. So the resemblance between the two types of flow may be strong but it is not quite perfect, and one should remain cautious as to how far the analogy can be stretched.
13. This backward velocity can be understood as follows: on the average, the cars in a dense jam occupy 7.5 m each, and they leave the front of the jam at a rate of one per 1.5 s (the combined reaction time of driver and car). So the front of the jam moves backward at a speed of 7.5 m per 1.5 s = 5 ms^{-1}, which is 18 km h^{-1}.

Notes on contributor

Ko van der Weele (1959) studied high energy physics with Nobel laureate Gerard 't Hooft (University of Utrecht, 1983), earned a Ph.D. in chaos theory from the University of Amsterdam in 1987, and got interested in granular matter around the year 2000 at the University of Twente in the Netherlands. Now at the University of Patras, Greece, he explores the borderline of granular and fluid dynamics – in the very fitting vicinity of a sandy beach.

References

[1] H. Jaeger, S. Nagel, and R. Behringer, *Granular solids, liquids, and gases*, Rev. Mod. Phys. 68 (1996), pp. 1259–1273.
[2] J. Duran, *Sand, Powders, and Grains: An Introduction to the Physics of Granular Materials*, Springer, New York, 2000.
[3] T.M. Knowlton, J.W. Carson, G.E. Klinzing, and W.C. Yang, *The importance of storage, transfer, and collection*, Chem. Eng. Prog. 90 (1994), pp. 44–54.
[4] E.F.F. Chladni, *Entdeckungen ueber die Theorie des Klanges*, Breitkopf und Härtel, Leipzig, 1787.
[5] M. Faraday, *On a peculiar class of acoustical figures; and on certain forms assumed by groups of particles upon vibrating elastic surfaces*, Philos. Trans. R. Soc. London 121 (1831), pp. 299–340.
[6] R.A. Bagnold, *The Physics of Blown Sand and Sand Dunes*, Methuen, London, 1941; reprinted by Dover Publ., Mineola, New York.
[7] M.A. Hopkins and M.Y. Louge, *Inelastic microstructure in rapid granular flows of smooth disks*, Phys. Fluids A 3 (1991), pp. 47–57.
[8] I. Goldhirsch and G. Zanetti, *Clustering instability in dissipative systems*, Phys. Rev. Lett. 70 (1993), pp. 1619–1622. See also I. Goldhirsch, *Clustering instability in granular gases*, in *Proc. DOE/NSF Workshop on Flow of Particulates and Fluids* Worcester MA, October 1991; S.I. Plasynski, W.C. Peters, and M.C. Roco, eds., National Technical Information Service, Springfield, VA, 1991, pp. 211–235.
[9] I. Goldhirsch, M.-L. Tan, and G. Zanetti, *A molecular dynamical study of granular fluids: the unforced granular gas*, J. Sci. Comput. 8 (1993), pp. 1–40.

[10] A. Kudrolli, M. Wolpert, and J.P. Gollub, *Cluster formation due to collisions in granular material*, Phys. Rev. Lett. 78 (1997), pp. 1383–1386.

[11] I. Goldhirsch, *Rapid granular flows*, Annu. Rev. Fluid Mech. 35 (2003), pp. 267–293.

[12] T. Pöschel, and N. Brilliantov (eds.), *Granular Gas Dynamics, Lecture Notes in Physics*, Springer, Berlin, 2003.

[13] M.C. Cross and P.C. Hohenberg, *Pattern formation outside of equilibrium*, Rev. Mod. Phys. 65 (1993), pp. 851–112.

[14] E. Bodenschatz, W. Pesch, and G. Ahlers, *Recent developments in Rayleigh–Bénard convection*, Annu. Rev. Fluid Mech. 32 (2000), pp. 709–778.

[15] J.L. Hansen, M. van Hecke, A. Haaning, C. Ellegaard, K. Haste Anderson, T. Bohr, and T. Sams, *Instabilities in sand ripples*, Nature 410 (2001), p. 324.

[16] V. Schwämmle and H.J. Herrmann, *Solitary wave behaviour of sand dunes*, Nature 426 (2003), pp. 619–620. H. Elbelrhiti, P. Claudin, and B. Andreotti, *Field evidence for surface-wave induced instability of sand dunes*, Nature 437 (2005), pp. 720–723.

[17] *Astronomy Picture of the Day: Sand Dunes Thawing on Mars* (3 March 2008). Available at http://antwrp.gsfc.nasa.gov/apod/ap080303.html.

[18] B. Thomas and A.M. Squires, *Support for Faraday's view of circulation in a fine-powder Chladni heap*, Phys. Rev. Lett. 81 (1998), pp. 574–577.

[19] H.J. van Gerner, MA.van der Hoef, D. van der Meer, and K. van der Weele, *Interplay of air and sand: Faraday heaping unraveled*, Phys. Rev. E 76 (2007), pp. 051305-1–7.

[20] M.-L. Tan and I. Goldhirsch, *Rapid granular flows as mesoscopic systems*, Phys. Rev. Lett. 81 (1998), pp. 3022–3025.

[21] J. Eggers, *Sand as Maxwell's demon*, Phys. Rev. Lett. 83 (1999), pp. 5322–5325.

[22] H.J. Schlichting and V. Nordmeier, *Strukturen im Sand*, Math. Naturwiss. Unterr. 49 (1996), pp. 323–332.

[23] J.C. Maxwell, *Theory of Heat*, Longmans, Green, London, 1871. The Demon is described in Chapter 12. Maxwell himself speaks of a 'very observant and neat-fingered being', the term 'Demon' was coined by William Thomson (the later Lord Kelvin) in 1874.

[24] A.S. Leff and A.F. Rex, *Maxwell's Demon: Entropy, Information, Computing*, Adam Hilger, Bristol, 1990. Resource Letter MD-1: Maxwell's Demon, Am. J. Phys. 58 (1990), pp. 201–209.

[25] S. McNamara and W.R. Young, *Inelastic collapse and clumping in a one-dimensional granular medium*, Phys. Fluids A 4 (1992), pp. 496–504.

[26] J.T. Jenkins and S.B. Savage, *A theory for the rapid flow of identical, smooth, nearly elastic, spherical particles*, J. Fluid Mech. 130 (1983), pp. 187–202. J.T. Jenkins and M.W. Richman, *Boundary conditions for plane flows of smooth, nearly elastic, circular disks*, Phys. Fluids 28 (1985), pp. 3485–3494.

[27] V. Kumaran, *Temperature of a granular material fluidised by external vibrations*, Phys. Rev. E 57 (1998), pp. 5660–5664.

[28] J.J. Brey, JW.Duffy, C.S. Kim, and A. Santos, *Hydrodynamics for granular flow at low density*, Phys. Rev. E 58 (1998), pp. 4638–4653.

[29] I.S. Aranson and L.S. Tsimring, *Patterns and collective behavior in granular media: Theoretical concepts*, Rev. Mod. Phys. 78 (2006), pp. 641–692.

[30] N.V. Brilliantov and T. Pöschel, *Kinetic Theory of Granular Gases*, Oxford University Press, Oxford, 2004.

[31] I. Ippolito, C. Annic, J. Lemaître, L. Oger, and D. Bideau, *Granular temperature: Experimental analysis*, Phys. Rev. E 52 (1995), pp. 2072–2075.

[32] P. Evesque, *Are temperature and other thermodynamic variables efficient concepts for describing granular gases and/or flows?*, Poudres & Grains 132 (2002), pp. 20–26.

[33] M. Hou, H. Tu, R. Liu, Y. Li, K. Lu, P.-Y. Lai, and C.K. Chan, *Temperature oscillations in a compartmentalized granular gas*, Phys. Rev. Lett. 100 (2008), pp. 068001-1–4.

[34] G.W. Baxter and J.S. Olafsen, *The temperature of a vibrated granular gas*, Granular Matter 9 (2007), pp. 135–139.

[35] A. Lipowski and M. Droz, *Urn model of separation of sand*, Phys. Rev. E 65 (2002), pp. 031307-1–7.

[36] F. Coppex, M. Droz, and A. Lipowski, *Dynamics of the breakdown of granular clusters*, Phys. Rev. E 66 (2002), pp. 011305-1–5.

[37] P. Ehrenfest and T. Ehrenfest, *The Conceptual Foundations of the Statistical Approach to Mechanics*, Dover, New York, 1990.

[38] F. Cecconi, A. Puglisi, U.M.B. Marconi, and A. Vulpiani, *Noise activated granular dynamics*, Phys. Rev. Lett. 90 (2003), pp. 064301-1–4.

[39] H.A. Kramers, *Brownian motion in a field of force and the diffusion model of chemical reactions*, Physica 7 (1940), pp. 284–304.

[40] P. Hänggi, P. Talkner, and M. Borkovec, *Reaction-rate theory: fifty years after Kramers*, Rev. Mod. Phys. 62 (1990), pp. 251–341.

[41] J.J. Brey, F. Moreno, R. García-Rojo, and M.J. Ruiz-Montero, *Hydrodynamic Maxwell demon in granular systems*, Phys. Rev. E 65 (2001), pp. 011305-1–4.

[42] K. van der Weele, R. Mikkelson, D. van der Meer, and D. Lohse, Cluster formation in compartmentalized granular gases, in *The Physics of Granular Media*, H. Hinrichsen, and D.E. Wolf, eds., Wiley-VCH, Weinheim, 2004, pp. 117–139.

[43] Y. Du, H. Li, and L. Kadanoff, *Breakdown of hydrodynamics in a one-dimensional system of inelastic particles*, Phys. Rev. Lett. 74 (1995), pp. 1268–1271.

[44] N. Sela and I. Goldhirsch, *Hydrodynamic equations for rapid flows of smooth inelastic spheres, to Burnett order*, J. Fluid Mech. 361 (1998), pp. 41–74.

[45] L. Kadanoff, *Built upon sand: theoretical ideas inspired by granular flows*, Rev. Mod. Phys. 71 (1999), pp. 435–444.

[46] P.G. Eshuis, *Colllective phenomena in vertically shaken granular matter*, Ph.D. thesis, University of Twente, Enschede, 2008.

[47] D. Lohse, R. Bergmann, R. Mikkelsen, C. Zeilstra, D. van der Meer, M. Versluis, K. van der Weele, M. van der Hoef, and H. Kuipers, *Impact on soft sand: Void collapse and jet formation*, Phys. Rev. Lett. 93 (2004), pp. 198003-1–4.

[48] P.G. Eshuis, K. van der Weele, M. van der Meer, and D. Lohse, *Granular Leidenfrost effect: Experiment and theory of floating particle clusters*, Phys. Rev. Lett. 95 (2005), pp. 258001-1–4.

[49] B. Meerson, T. Pöschel, and Y. Bromberg, *Close-packed floating clusters: granular hydrodynamics beyond the freezing point?*, Phys. Rev. Lett. 91 (2003), pp. 024301-1–4.

[50] Y. Forterre and O. Pouliquen, *Longitudinal vortices in granular flows*, Phys. Rev. Lett. 86 (2001), pp. 5886–5889.
[51] Y. Forterre and O. Pouliquen, *Stability analysis of rapid granular chute flows: formation of longitudinal vortices*, J. Fluid Mech. 467 (2002), pp. 361–387.
[52] E. Khain and B. Meerson, *Onset of thermal convection in a horizontal layer of granular gas*, Phys. Rev. E 67 (2003), pp. 021306-1–6.
[53] P. Eshuis, et al. *Buoyancy-driven granular convection: experiment, theory, and numerical simulation*, Ph.D. thesis, University of Twente, Enschede, 2008.
[54] E.L. Grossman, T. Zhou, and E. Ben-Naim, *Towards granular hydrodynamics in two dimensions*, Phys. Rev. E 55 (1997), pp. 4200–4206.
[55] S. Luding, *Global equation of state of twodimensional hard sphere systems*, Phys. Rev. E 63 (2001), pp. 042201-1–4.
[56] O. Herbst, P. Müller, M. Otto, and A. Zippelius, *Local equation of state and velocity distributions of a driven granular gas*, Phys. Rev. E 70 (2004), pp. 051313-1–14.
[57] P. Jean, H. Bellenger, P. Burban, L. Ponson, and P. Evesque, *Phase transition or Maxwell's demon in granular gas?* Poudres & Grains 13 (2002), pp. 27–39.
[58] R. Mikkelsen, K. van der Weele, D. van der Meer, M. van Hecke, and D. Lohse, *Small-number statistics near the clustering transition in a compartmentalized granular gas*, Phys. Rev. E 71 (2005), pp. 041302-1–12.
[59] K. van der Weele, D. van der Meer, M. Versluis, and D. Lohse, *Hysteretic clustering in granular gas*, Europhys. Lett. 53 (2001), pp. 328–334.
[60] P.M. Chaikin and T.C. Lubensky, *Principles of Condensed Matter Physics*, Cambridge University Press, Cambridge, 1995.
[61] D. van der Meer, K. van der Weele, and D. Lohse, *Bifurcation diagram for compartmentalized granular gases*, Phys. Rev. E 63 (2001), pp. 061304-1–9.
[62] U. Marini Bettolo Marconi and M. Conti, *Dynamics of vibrofluidised granular gases in periodic structures*, Phys. Rev. E 69 (2004), pp. 011302-1–8.
[63] D. van der Meer, K. van der Weele, and D. Lohse, *Coarsening dynamics in a vibrofluidised compartmentalized granular gas*, J. Stat. Mech. April (2004), pp. P04004-1–29.
[64] K. van der Weele, D. van der Meer, and D. Lohse, *Ultraslow coarsening in compartmentalized granular gases*, J. Nonlinear Phenom. Complex Syst. 10 (2007), pp. 116–126.
[65] D. van der Meer, K. van der Weele, P. Reimann, and D. Lohse, *Compartmentalized granular gases: flux model results*, J. Stat. Mech. July (2007), pp. P07021-1–28.
[66] D. van der Meer, K. van der Weele, and D. Lohse, *Sudden collapse of a granular cluster*, Phys. Rev. Lett. 88 (2002), pp. 174302-1–4.
[67] D. van der Meer and K. van der Weele, *Breakdown of a near-stable granular cluster*, Prog. Theor. Phys. Suppl. 150 (2003), pp. 297–311.
[68] D. van der Meer, P. Reimann, K. van der Weele, and D. Lohse, *Spontaneous ratchet effect in a granular gas*, Phys. Rev. Lett. 92 (2004), pp. 184301-1–4.
[69] D. van der Meer, K. van der Weele, and P. Reimann, *Granular fountains: convection cascade in a compartmentalized granular gas*, Phys. Rev. E 73 (2006), pp. 061304-1–12.
[70] F. Jülicher and J. Prost, *Cooperative molecular motors*, Phys. Rev. Lett. 75 (1995), pp. 2618–2621.
[71] P. Reimann, R. Kawai, Van den Broeck, and P. Hänggi, *Coupled Brownian motors: anomalous hysteresis and zero-bias negative conductance*, Europhys. Lett. 45 (1999), pp. 545–551.
[72] P. Reimann, *Brownian motors: noisy transport far from equilibrium*, Phys. Rep. 361 (2002), pp. 57–265.
[73] R. Mikkelsen, D. van der Meer, K. van der Weele, and D. Lohse, *Competitive clustering in a bidisperse granular gas*, Phys. Rev. Lett. 89 (2002), pp. 214301-1–4.
[74] A. Barrat and E. Trizac, *A molecular dynamics 'Maxwell Demon' experiment for granular mixtures*, Mol. Phys. 101 (2003), pp. 1713–1719.
[75] R. Lambiotte, J.M. Salazar, and L. Brenig, *From particle segregation to the granular clock*, Phys. Lett. A 343 (2005), pp. 224–230.
[76] G. Constantini, D. Paolotti, C. Cattulo, and U.M.B. Marconi, *Bistable clustering in driven granular mixtures*, Physica A 347 (2005), pp. 224–228.
[77] S. Viridi, M. Schmick, and M. Markus, *Experimental observations of oscillations and segregation in a binary granular mixture*, Phys. Rev. E 74 (2006), pp. 041301-1–4.
[78] S. Viridi, *Granulare Medien und stochastische Resonanz in Zwei-Kammer-Systemen*, Ph.D. thesis, University of Dortmund, 2007.
[79] P. Evesque, *Cyclic Maxwell demon in granular gas using 2 kinds of spheres with different masses*, Poudres & Grains 162, (2007), pp. 23–37.
[80] J.L. Spradley, *Velocity amplification in vertical collisions*, Am. J. Phys. 55 (1987), pp. 183–184.
[81] R. Mikkelsen, D. van der Meer, K. van der Weele, and D. Lohse, *Competitive clustering in a granular gas*, Phys. Fluids 159, (2003), p. S8.
[82] R. Mikkelsen, D. van der Meer, K. van der Weele, and D. Lohse, *Competitive clustering in a bidisperse granular gas: experiment, Molecular Dynamics, and Flux Model*, Phys. Rev. E 70 (2004), pp. 061307-1–12.
[83] E.K.O. Hellén and J. Krug, *Coarsening of sand ripples in mass transfer models*, Phys. Rev. E 66 (2002), pp. 011304-1–9.
[84] D.E. Wolf, M.E. Schreckenberg, and A. Bechem (eds.), *Traffic and Granular Flow*, World Scientific, Singapore, 1996. M.E. Schreckenberg and D.E. Wolf (eds.), *Traffic and Granular Flow '97*, Springer, Singapore, 1998; D. Helbing et al. (eds.), *Traffic and Granular Flow '99*, Springer, Berlin, 2000; M. Fukui et al. (eds.), *Traffic and Granular Flow '01*, Springer, Berlin, 2003; S.P. Hoogendoorn, S. Luding, and D.E. Wolf (eds.), *Traffic and Granular Flow '03*, Springer, Berlin, 2006.
[85] D. Helbing, *Traffic and related self-driven many-particle systems*, Rev. Mod. Phys. 73 (2001), pp. 1067–1141.
[86] K. van der Weele, W. Spit, T. Mekkes, and D. van der Meer, From granular flux model to traffic flow description, in *Traffic and Granular Flow '03*, S.P. Hoogendoorn, S. Luding, P.H.L. Bovy, M. Schreckenberg, and D.E. Wolf, eds., Springer, Berlin, 2005, pp. 569–578.
[87] D. Chowdhury, L. Santen, and A. Schadschneider, *Statistical physics of vehicular traffic and some related systems*, Phys. Rep. 329 (2000), pp. 199–329.
[88] D. Helbing, A. Hennecke, and M. Treiber, *Phase diagram of traffic states in the presence of inhomogeneities*, Phys. Rev. Lett. 82 (1999), pp. 4360–4363.
[89] B.S. Kerner, S.L. Klenov, and D.E. Wolf, *Cellular automata approach to threephase traffic flow*, J. Phys. A: Math. Gen. 35 (2002), pp. 9971–10013.